Developments in the Built Environment 23 (2025) 100736

Contents lists available at ScienceDirect

Developments in the Built Environment

journal homepage: www.sciencedirect.com/journal/developments-in-the-built-environment

Compressive strength prediction of fly ash/slag-based geopolymer concrete using EBA-optimised chemistry-informed interpretable deep learning model

Yang Yu [a,*], Iman Munadhil Abbas Al-Damad [a,b], Stephen Foster [a,**], Ali Akbar Nezhad [a,c], Ailar Hajimohammadi [a,***]

[a] Centre for Infrastructure Engineering and Safety, School of Civil and Environmental Engineering, The University of New South Wales, Sydney, NSW, 2052, Australia
[b] Department of Civil Engineering, College of Engineering, University of Baghdad, Iraq
[c] Boral Ltd, North Ryde, NSW, 2113, Australia

ARTICLE INFO

Keywords:
Chemistry-informed
Compressive strength
Convolutional neural network
Enhanced bat algorithm
Geopolymer concrete

ABSTRACT

Geopolymer concrete (GPC) is a sustainable alternative to conventional Portland cement concrete, utilising industrial by-products like fly ash (FA) and ground-granulated blast-furnace slag (GGBS). However, optimising GPC's compressive strength (CS) often requires costly and time-consuming experimental trials. This study develops a deep learning (DL) model based on convolutional neural networks (CNN) to predict the CS of FA/GGBS-based GPC. The model integrates key mix parameters such as material proportions, curing conditions, and the chemical composition of FA/GGBS binders, making it chemistry-informed. The CNN architecture includes two convolution layers, global max-pooling, and two fully connected layers, with 11 input variables and a single output for CS prediction. To optimise model accuracy, the enhanced bat algorithm (EBA) is designed for metaparameter tuning. The model is trained and tested on a comprehensive dataset comprising experimental data extracted from published literature. The results demonstrate that the EBA-optimised CNN outperforms traditional learning models, including support vector machine (SVM), extreme gradient boosting (XGBoost), and artificial neural networks (ANN), with higher performance in terms of R^2, MAE, and RMSE. The model achieved R^2 values of 0.997 for training and 0.978 for testing. Additionally, the Shapley additive explanations (SHAP) method was used to interpret the model, identifying the Na_2O to binder ratio and curing age as the most influential factors on CS. This study highlights the potential of DL techniques, particularly chemistry-informed CNN with metaparameter optimisation, for accurately predicting the strength of GPC, providing a cost-effective solution for mix design and performance evaluation.

1. Introduction

Geopolymer concrete (GPC) is a type of concrete that uses by-products and alkaline activators instead of Portland cement to bind the aggregate together (Bahmani et al., 2024). The paste is typically made from a mixture of an alkali source (such as sodium hydroxide or potassium hydroxide) and an aluminosilicate source (such as fly ash, slag, or kaolin) (Jia et al., 2020; Shilar et al., 2022; Wang et al., 2025; Xiao et al., 2022; Zhou et al., 2024a). This results in a material that is more sustainable, environmental-friendly, and has improved mechanical properties (e.g., compressive strength, elastic modulus, splitting tensile strength and flexural strength) and durability (e.g., shrinkage, fire resistance, sulfate resistance and chloride penetration resistance) compared to traditional Portland cement concrete (Siddika et al., 2021; Zhou et al., 2024c). The production of GPC also generates less carbon dioxide emission, making it a more sustainable alternative for construction (Gao et al., 2025a; Kanagaraj et al., 2024). Among the various available geopolymer materials, fly ash (FA) and ground-granulated

This article is part of a special issue entitled: Novel Materials Testing published in Developments in the Built Environment.

* Corresponding author.
** Corresponding author.
*** Corresponding author.
E-mail addresses: yang.yu12@unsw.edu.au (Y. Yu), s.foster@unsw.edu.au (S. Foster), ailar.hm@unsw.edu.au (A. Hajimohammadi).

https://doi.org/10.1016/j.dibe.2025.100736
Received 10 May 2025; Received in revised form 7 August 2025; Accepted 13 August 2025
Available online 20 August 2025

blast-furnace slag (GGBS) have become the preferred options; this is due to their relative abundance and their silica and alumina content (Li et al., 2022; Shilar et al., 2023b; Shilar et al., 2025; Zhang, B. et al., 2025). Hardjito and Rangan (2005) designed low-calcium FA-based GPC, the properties of which were also analysed via experiments. Ng and Foster (2013) explored a design approach to achieve ideal combination of GPC with a particular emphasis on enhancing compressive strength, where FA and GGBS were employed as primary components in producing GPC binder. In the design of GGBS/FA-based GPC, strength is a primary mechanical property considered in design (Amin, M. et al., 2022; Shilar et al., 2023a; Zhang et al., 2024). It is typically determined through testing after a standard 28-day curing period (Zhou et al., 2024b). However, the 28-day waiting time can hinder timely mix development and mix optimisation, where a wide array of materials and precursors are available (Gao et al., 2025b). As a result, there has been significant interest from both academia and industry in developing a reliable predictive model for the estimation of strength prior to mix development and testing.

A variety of models have been proposed to predict compressive strength of GPC and mortar. For example, Cong et al. (2020) developed a model to predict the properties of GGBS/FA GPC based on stress-strain and modulus of elasticity under combined tension and compression loading. However, the model predictions were not consistent with test results. Zhang et al. (2020) analysed the residual strength of low calcium FA-based GPC after high-temperature exposure and found that the experimental strengths were usually higher than the predicted values. Le et al. (2021) compared the revised Feret model (2019) and De Larrard model (1999) to predict the strength of FA-based geopolymer recycled aggregate concrete, with De Larrard model giving satisfactory results with only natural and recycled aggregate parameters determined in advance. A disadvantage of these models is that the calculation process solidifies the expression of the function, limiting the possibility of further improving prediction accuracy. For geopolymer binders, Ng and Foster (2013) developed a performance matrix-based approach on a mix of fly ash and slag, with consideration to particle packing density. While this approach is useful in optimising mix design using a given set of materials for strength, it is experimentally intensive (and thus time-costly).

In recent years, artificial intelligence in concrete mix design and performance prediction has been getting significant attention (Alyami et al., 2024; Wu et al., 2024; Zandifaez et al., 2023). Using machine learning (ML) in place of empirical methods for predicting concrete mechanical properties is advantageous due to its ability to account for nonlinear relationships between variables, together with the impact of other factors (Ai et al., 2022; Liu et al., 2024). Most ML algorithms divide data into training and testing sets and iterate until predictions meet requirements (Zhang et al., 2023; Zhang, T. et al., 2025), whereas empirical models can only iterate once, resulting in fitting parameters. This explains why simple regression often fails to deliver desired results. In the field of ML-based strength prediction of GPC, Ahmad et al. (2022) conducted a study to compare the accuracy of three ML methods: decision tree (DT), AdaBoost, and bagging regressor (BR). The study aimed to predict the compressive strength of GPC, which includes FA. The results showed that the BR method had the highest accuracy among the methods tested. To improve prediction accuracy of strength for possible lower effect alternative to Portland cement mixes, Peng and Unluer (2022) utilised three ML methods to evaluate 28-day compressive strength of FA-based GPC; namely, support vector machine (SVM), artificial neural networks (ANN) and extreme learning machine (ELM). Gunasekara et al. (2021) proposed a hybrid model, consisting of ANN, Levenberg-Marquardt (LM) algorithm and Bayesian regularisation algorithm to characterise modulus of elasticity and tensile strength of high-calcium FA-based GPC, in which compressive strength is included as a model input. In Awoyera et al. (2020), tensile strength and flexural strength of GPC were modelled using ANN and genetic expression programming (GEP), where FA was substituted for silica fume and GGBS, in addition to sand. A comparative study on the capabilities of different ML approaches in modelling strength of GGBS/FA-based GPC was conducted by Gupta and Rao (2022). However, the comparison results demonstrated that prediction accuracy of these models is significantly impacted by input variable selection and model metaparameter setting.

The advancement of deep learning (DL) has revolutionised various fields in recent years, making it possible to tackle complex problems that were once not possible (Ai et al., 2023; Jiang et al., 2024). The combination of feature extraction and pattern recognition in DL has enabled the creation of highly sophisticated models capable of performing complex tasks with high accuracy. Some of the areas where DL has been applied include computer vision, natural language processing, fraud detection, video streaming, transportation, etc. In the fields of concrete materials and structures, DL has also been utilised to address a variety of challenges. Damage diagnosis of concrete beams, for example, can be performed using a deep stacked autoencoder (SAE) network-based framework, as proposed by Yu et al. (2023). In their work, they employed principal component analysis (PCA) technique to extract features from the frequency responses of vibration measurements, which were then used as inputs to the deep SAE network. Jo and Jadidi (2020) utilised deep belief networks to develop an automated classification system, which can be installed on unmanned aerial vehicles (UAV) to analyse RGB and infrared images for surface crack detection of concrete structures. On basis of generative adversarial network, Dunphy et al. (2022) proposed a deep transfer learning framework for multiple damage classification of concrete structure. In Yu et al. (2022), deep CNN models (i.e., AlexNet and GoogLeNet) were utilised for concrete crack detection and segmentation, which demonstrated outstanding performance despite the input images being polluted with various noises. CNN was also employed for evaluating workability properties of concrete, such as slump and slump flow, based on video captured during concrete mix procedure (Yang et al., 2021). Deng et al. (2018) employed CNN to develop a predictive model to estimate strength of recycled aggregate concrete, where the network input was in the form of 2×2 matrix containing water-cement ratio, fine aggregate replacement ratio, coarse aggregate replacement ratio and FA content (Oyebisi and Alomayri, 2023). explored the application of deep neural networks (DNN) to predict mechanical strengths of GPC made of corncob ash (CCA) and GGBS. The results showed that a 10-20-20-20-1 network topology was most effective for predicting compressive and flexural strengths, while a 10-17-17-17-1 topology was best for split tensile strength. Among various DL methods, CNN, with remarkable ability to generalise, has been widely applied in concrete field. However, the performance of CNN is inextricably linked to the arrangement of its metaparameters, which act as a guide for training the network. Altering these metaparameters can produce remarkably diverse results for a CNN. Although a set of metaparameters may prove to be successful in one scenario, it may not yield the same level of performance in other situations. Thus, it is important to optimise the parameters of a CNN prior to utilising it in a specific application.

The primary objective of this study is to develop a chemistry-informed and interpretable DL model for predicting the compressive strength of GPC containing FA and GGBS. Recent advancements in ML/DL have demonstrated great potential in capturing complex and nonlinear relationships between input variables and output predictions. However, existing models often fail to account for the diverse chemical compositions and blend proportions of GGBS/FA binders, which significantly influence strength. This study adopts 1D-CNN to incorporate not only the mix proportions and curing conditions but also the chemical makeup of the GGBS/FA blends. The model architecture consists of two convolution layers, followed by a global max-pooling layer and two fully connected layers. To enhance model accuracy and generalisation, the CNN metaparameters are optimised using the enhanced bat algorithm (EBA) that improves convergence and solution quality over standard methods. The specific objectives of this research are:

- To develop a robust DL model that integrates both the mix proportions and the chemical composition of GGBS/FA blends for more accurate compressive strength prediction.
- To optimise the metaparameters of the CNN using EBA to enhance the model accuracy.
- To interpret the model's predictions by identifying and quantifying the influence of each input variable on the compressive strength of GPC, using Shapley additive explanations (SHAP).

2. Theoretical background

2.1. D convolutional neural network

1D-CNN is a type of convolutional neural network for dealing with sequential data (Nguyen et al., 2023). In 1D-CNN, the input, convolutional kernel and outputs of convolution and pooling layers are all one-dimensional, which is different from that of 2D-CNN. Since 1D-CNN adopts an end-to-end network structure, it is highly robust. Like 2D-CNN, 1D-CNN also contains the characteristics of local connectivity and weight sharing, where local connectivity utilises spatial topology to establish non-fully connected spatial relationships between neighbouring layers to reduce the number of parameters required to train the network, and weight sharing is used to avoid the overfitting of trained model. In general, 1D-CNN is composed of an input layer, convolution layers, pooling layers, fully connected (FC) layers, and an output layer.

The function of convolution layer is to extract features from input data to perform a local convolution operation on the target input by sequentially sliding a convolution kernel, which is essentially a weight matrix learned by a local sensory field. The main feature of convolution layer is the utilisation of local connectivity and weight sharing. The one-dimensional convolutional operation is expressed as:

$$y^i = f\left(\sum_i k^{ij} * x^i + b^i\right) \tag{1}$$

where "*" denotes the convolutional operation; y^i denotes ith output feature map; x^i denotes ith input feature map; k^{ij} denotes the convolution kernel; b^i denotes the bias of ith feature map; $f(\cdot)$ denotes the activation function. In CNN, there are several activation functions to be selected for conducting nonlinear transformation, including hyperbolic tangent function (tanh), sigmoid function, rectified linear unit (ReLU) and leaky ReLU (LReLU). The expression of four nonlinear activation functions is summarised in Fig. 1.

The pooling layer has the main function of removing redundant information to extract important features while maintaining feature consistency, which can help prevent overfitting. There are two commonly used pooling methods: maximum pooling and average pooling, which can be represented by:

$$p^l = \max\{a^l\} \tag{2}$$

$$p^l = \frac{l}{k}\sum a^l \tag{3}$$

where p denotes the feature matrix obtained by pooling, l denotes the width of feature map, and a denotes the feature matrix after activation of convolution layer. Maximum pooling and average pooling calculate the maximum and mean values within adjacent rectangular regions, respectively; maximum pooling is more commonly used owing to its location-independent information.

The FC layer is used to comprehensively fuse the local features extracted from convolution and pooling layers to obtain all the features of input data. It is the same as the hidden layer in back-propagation (BP) neural network. Based on combined features, the prediction result will be generated using a regression activation function.

2.2. Bat algorithm

The bat algorithm (BA) is a stochastic search algorithm that simulates the ability of bats to detect and pursue prey and avoid obstacles using ultrasonic echolocation, thus correlating it with the global search function (Yang and Hossein Gandomi, 2012). The fundamental of BA is to map a population of N individual bats to NP feasible solutions in D-dimensional space, modelling the optimisation process as prey detection and search by individual bats in the population. In the optimisation process, each individual bat changes its location by adjusting its own loudness and pulse rate, evaluating the superiority and inferiority of location according to fitness value, and replacing inferior solution with better one, thus following the optimal individual bat and finding the global optimal solution. In a D-dimensional space, the updating of velocity and location of ith bat can be formulated as:

$$f_i = f_{min} + (f_{max} - f_{min})\beta \tag{4}$$

$$v_i^{t+1} = v_i^t + (x_i^t - x^*)f_i \tag{5}$$

$$x_i^{t+1} = x_i^t + v_i^t \tag{6}$$

where f_i denotes pulse frequency of ith bat; f_{max} and f_{min} denote the maximum and minimum pulse frequencies, respectively; x_i^t denotes the location of ith bat at time t; v_i^t denotes the velocity of ith bat at time t; x^*

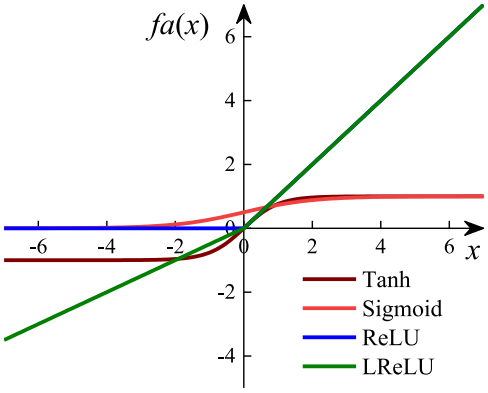

Name	Expression
Tanh	$fa(x) = \frac{e^x - e^{-x}}{e^x + e^{-x}}$
Sigmoid	$fa(x) = \frac{1}{1 + e^{-x}}$
ReLU	$fa(x) = \max(0, x)$
LReLU	$fa(x) = \begin{cases} \vartheta x, x < 0 \\ x, x \geq 0 \end{cases}$

Fig. 1. Comparisons of different activation functions.

is the optimal solution among all individuals in the current iteration; β is a random number between 0 and 1.

During the local search process, the random walk is performed on the current optimal solution and a new optimal solution is generated. The formula of local search for optimal solution is given by:

$$x_{new} = x_{pre} + \varepsilon A^t \tag{7}$$

where x_{pre} denotes the previous optimal solution; x_{pre} is newly generated optimal solution after random walk; ε is a random number between 0 and 1; A^t denotes the mean loudness of the whole population at time t.

In the initial stage of iterative search, the bats emit pulses with low frequencies and high loudness to extend the search range and enhance the global search ability of algorithm. When the approximate area of global optimum is localised, the loudness is reduced, and pulse emission rate is gradually increased to raise the local search ability to improve the solution accuracy. The updated formulae of loudness A_i^{t+1} and pulse emission rate R_i^{t+1} of ith bat are provided as follows:

$$A_i^{t+1} = \alpha A_i^t \tag{8}$$

$$R_i^{t+1} = R_i^0(1 - e^{-\gamma t}) \tag{9}$$

where A_i^t and R_i^t denote the loudness and pulse emission rate of ith bat at time t; α is a random number between 0 and 1; γ denotes pulse emission rate enhancement coefficient, which is above 0.

3. Dataset development and analysis

It is well known that a consolidated experimental database, which comprises all the influencing variables, is of great significance for the development of a highly accurate and robust data-driven surrogate model to predict compressive strength of GGBS/FA-based GPC. To ensure the reliability and relevance of the data used in this study, a systematic literature review was conducted following preferred reporting items for systematic reviews and meta-analyses (PRISMA) guideline. First, relevant studies were identified through a comprehensive search of major databases, including Web of Science, Scopus and Google Scholar. The search was conducted using keywords, such as geopolymer concrete, fly ash, GGBS and compressive strength. Initially, more than 900 groups of experimental data of GGBS/FA-based GPC of oven and ambient cured GPC concrete, of different mixes, and ages, were collected from 22 scientific papers published between 2001 and 2022 (Castel and Foster, 2015; Chithambaram et al., 2018; Das and Shrivastava, 2021; Deb et al., 2014, 2015; Fang et al., 2018; Jithendra and Elavenil, 2019; Karthik et al., 2017; Lee and Lee, 2013; Memon et al., 2011; Morsy et al., 2022; Nath and Sarker, 2017; Noushini et al., 2016, 2020; Pavithra et al., 2016; Reddy et al., 2013; Roy et al., 2022; Tang et al., 2019; Upreti et al., 2022; Verma and Dev, 2021, 2022; Waqas et al., 2021).

In low-calcium GGBS/FA blended binders, a minimum volume of calcium silicate derived from the slag is needed to achieve practical strengths for structural concrete (characteristic strengths of 25 MPa and higher), without the use of externally applied heat (Davidovits, 2008; Kumar et al., 2010; Lee and Lee, 2013). In addition, the strength of blends with low volumes of slag can vary greatly depending on the preparation, condition, and properties of the activator and of the source materials (Davidovits, 2008). It is well recognised that the geopolymerisation potential of FA is highly dependent on its source. Fly ashes with high glass content are more conducive to polymerisation, while those containing high levels of disruptive species can significantly slow down the reactions, potentially rendering the final product non-viable as a cementitious material replacement (Davidovits, 2008). The GGBS-to-total binder ratio of 0.3 for ambient is adopted based on experimental evidence demonstrating that slag content below 30 % fails to provide adequate calcium for strength-forming C-A-S-H gel under ambient condition, resulting in inconsistent setting and subpar mechanical properties (Lee and Lee, 2013; Nath and Sarker, 2014). Conversely, for oven-cured specimens, elevated temperature accelerates the dissolution and reaction of fly ash aluminosilicates, reducing the reliance on calcium from slag. Here, a lower threshold of 0.1 suffices, as validated by studies confirming that heat curing enables viable geopolymerisation even with minimal slag content (Pavithra et al., 2016; Morsy et al., 2022). It is taken *a priori* that only fly ashes meeting minimum requirements for polymerisation are incorporated into the mix, such as those defined according to criteria established in Fernández-Jiménez and Palomo (2003) and Duxson et al. (2007), and summarised in Davidovits (2008).

Furthermore, all the experimental results employed standardised measurement techniques, primarily following ASTM C39 or equivalent protocols for compressive strength testing. Variations in specimen geometry, such as cube versus cylinder tests, were addressed by applying a conversion factor of 0.85 to cube strength to ensure consistency with cylinder-based prediction, as adopted by Yi et al. (2006). Sample preparation protocols were rigorously reviewed: all included studies documented curing conditions ranging from ambient temperatures of 15–30 °C to oven curing at 60–120 °C, standard mould types, including steel or plastic, and consistent mixing procedures such as controlled alkali activator-to-binder ratios. Quality control measures involved cross-verification of extracted data by the first and second authors and exclusion of studies with incomplete methodological details, such as undocumented curing humidity or activator purity. This harmonisation ensured the dataset reflected reproducible, high-confidence experimental outcomes while minimising bias from heterogeneous protocols.

Finally, the dataset, comprising a total of 376 groups of experimental data, is obtained for establishing a strength prediction model of GGBS/FA-based GPC. The exclusions are based on several key factors. First, only mixes meeting minimum GGBS-to-binder ratios of 0.3 for ambient curing or 0.1 for oven curing are retained to ensure structural viability, as supported by prior research from Davidovits (2008). Second, fly ash samples that do not satisfy established polymerisation criteria regarding glass content and chemical composition are excluded, following the work of Fernández-Jiménez and Palomo (2003) and Duxson et al. (2007). Third, data lacking standardised compressive strength testing protocols such as ASTM C39 or equivalent, or involving uncorrected specimen geometries, are removed to maintain consistency. Fourth, studies with incomplete methodological details, such as undocumented curing conditions or missing mix parameters, are omitted to ensure reproducibility. Additionally, it is worth noting that in Karthik et al. (2017), bio-additives were used in the geopolymer concrete mix, while in Tang et al. (2019), recycled aggregates were incorporated into the mix. During the data collection process, only the reference mix cases in both references were considered, which did not include either bio-additives or recycled aggregates, as these are outside the scope of this study. This rigorous filtering process, while substantially reducing the dataset size, ensures homogeneity and reliability, aligning the data with the study's objectives and minimising biases from inconsistent experimental protocols. The final curated dataset thus represents high-quality, reproducible results suitable for robust model development. Table 1 provides a summary of the studies included in the dataset, together with the number of data points extracted from each study and the key variables included. Fig. 2 presents the flowchart outlining data sources, collection, screening, refining and analysis process. The detailed information about the dataset is also available in the Supplementary Materials.

The variables in the dataset not only comprises constituent materials, curing conditions and measurements, including FA, GGBS, ratio of fine aggregate to binder (FBR), ratio of coarse aggregate to binder (CBR), ratio of water to solid (W/S), superplasticiser (SP), curing temperature (CT), oven curing hour (CH), concrete age (CA) and compressive strength (CS), but also includes the parameters related to chemical compositions of FA/GGBS blended binders, such as molar ratio (Ms) of silicon dioxide (SiO_2) to sodium oxide (Na_2O) and ratio of Na_2O to

Table 1
Summary of experimental dataset collected from literature.

Reference	No of data samples	Key variables
Lee and Lee (2013)	5	FA, GGBS, alkaline solution
Upreti et al. (2022)	45	FA, GGBS, curing condition
Karthik et al. (2017)	6	FA, GGBS, alkaline solution, bio-additives, curing duration
Verma and Dev (2021)	50	FA, GGBS, alkaline solution, curing duration
Jithendra and Elavenil (2019)	10	GGBS, superplasticiser, curing duration
Tang et al. (2019)	3	FA, GGBS, recycled aggregate replacement ratio, curing condition
Roy et al. (2022)	34	FA, GGBS, alkaline solution, curing condition
Morsy et al. (2022)	60	FA, GGBS, alkaline solution, curing temperature
Das and Shrivastava (2021)	6	FA, GGBS, alkaline solution, curing condition
Fang et al. (2018)	5	FA, GGBS, alkaline solution
Waqas et al. (2021)	60	FA, GGBS, alkaline solution, aggregate, curing duration
Verma and Dev (2022)	44	Liquid to binder ratio, curing temperature, alkaline solution
Noushini et al. (2020)	48	FA, GGBS, curing condition

binder (nm). Although inherent variations in FA fineness, specific glass content, or minor impurities within the defined criteria remain, the model directly accounts for the resulting activator chemistry used with these binders. As critical variables of model, Ms and nm capture the effective alkalinity and silicate modulus driving the geopolymerisation reaction in the specific mix, thereby allowing the model to adapt to variations in the inherent reactivity of the source materials used across different studies included in the dataset. Table 2 displays the results of statistical analysis of these variables in the database, comprising maxima (Max), minima (Min), median, mode, mean, range, skewness, kurtosis, and standard deviation (Std). Among these statistical metrics, median, mode and mean indicate the central characteristics of data, whereas Max, Min, range, skewness, kurtosis and Std relate to irregular characteristics of data. Since the statistical results demonstrate wider ranges of influencing parameters of strength of GGBS/FA-based GPC, the robustness of designed data-driven model can be guaranteed for further practical applications. Fig. 3 portrays relative frequency distributions (RFD) and cumulative percents of all the parameters in the database via the column diagrams. The RFD describes the percentage of total observations related to each value range, which corresponds to probability distributions utilised in statistics.

The influence of each parameter on strength of GGBS/FA-based GPC is analysed based on the previous studies. It is well known that in the blended system, where ambient curing is applied, increasing FA amount will decrease the strength of GPC (Castel and Foster, 2015; Hajimohammadi et al., 2019; Nath and Sarker, 2014). The GGBS, however, contributes to the improvement of strength of GPC. On the other hand, studies showed that increasing the slag content reduces the setting time and increases shrinkage (Lemougna et al., 2020). Nedeljković et al. (2018) concluded that lower slag contents, 30 % and 50 %, exhibited better workability and lower autogenous shrinkage. On the one hand, the study by Yadollahi et al. (2015) showed that strength increases with the increase of Na_2O content from 4 % to 10 % and with silica modulus increase from 0.52 to 0.68; on the other hand, the strength decreases with increasing water/binder ratio from 0.36 to 0.44. Other researchers supported that decreasing water to binder ratio leads to an increase of strength (Allahverdi et al., 2008; Bakharev, 2005; Hajimohammadi et al., 2017; Luukkonen et al., 2020; Van Jaarsveld et al., 2002). In another study, Firdous and Stephan (2019) showed that low silica modulus of alkaline solution leads to efflorescence and a lower degree of polymerisation, thus reducing compressive strength. While at higher

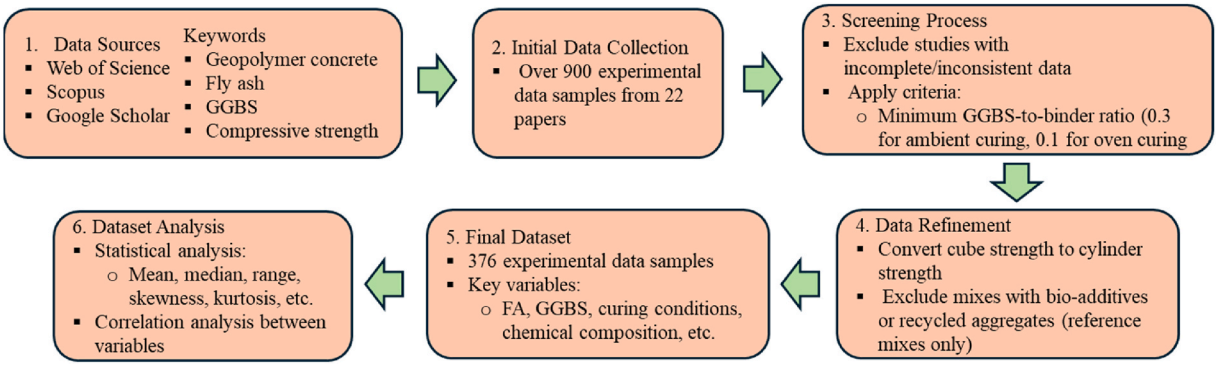

Fig. 2. Flowchart of the process of data sources, collection, screening, refining and analysis.

Table 2
Statistical metrics of dataset for GGBS/FA-based GPC compressive strength prediction.

Parameter	Metrics								
	Max	Min	Median	Mode	Mean	Range	Skewness	Kurtosis	Std
FA (kg/m^3)	378	0	287	304	248	378	−1.44	4.13	101
GGBS (kg/m^3)	450	38.8	120	101	156	411	1.32	3.97	102
FBR	2.33	1.31	1.69	1.69	1.68	1.02	1.58	9.18	0.143
CBR	3.95	2.27	3.13	3.13	3.06	1.68	−0.893	5.67	0.260
W/S	0.507	0.136	0.259	0.507	0.301	0.371	0.865	2.42	0.106
Ms	1.63	0.532	0.977	0.678	0.971	1.10	0.398	2.22	0.274
nm (%)	23.7	4.32	7.96	7.96	9.95	19.3	1.91	5.11	5.48
SP (%)	6.00	0	0	0	0.524	6.00	2.64	13.7	0.881
CT (°C)	120	15.0	60.0	60.0	51.2	105	0.279	2.32	23.0
CH (h)	48.0	0	24.0	24.0	18.7	48.0	0.411	2.17	16.5
CA (day)	90.0	1.00	28.0	28.0	24.7	89.0	1.16	4.63	19.3
CS (MPa)	76.2	11.9	31.0	45.9	35.8	64.3	0.541	2.31	14.5

silica modulus, the strength reduces again. This is due to the dissolution of aluminate and silicate species that increases with the reduction of silica modulus, and at higher silica modulus, the dissolution of the raw sample decreases. However, the mechanical properties of the resultant gel formed depend on the degree of polymerisation of the gel structure. Firdous and Stephan (2019) concluded that the optimum silica moduli depend on the composition of natural pozzolan. In a study by Kaze et al. (2021), it was found that the optimum silica modulus is about 1.3 and increasing the silica modulus further had a detrimental effect on the hardened properties of alkali-activated binder. Given the discussion above, it is concluded that no clear relationship is observable between silica modulus, or Na_2O content, and strength. Rather, it is dependent on the binder properties (Adewumi et al., 2021; Allahverdi et al., 2008; Luukkonen et al., 2020).

The above analysis shows that the compressive strength of GGBS/FA-based GPC is influenced by a variety of factors, in different ways. Accordingly, all these influencing factors need to be considered in strength prediction model development. In view of this, each input of surrogate model is supposed to be independent of others to prevent information from being redundant, which may lower the generalisation capacity of developed model. In this section, the independence of influencing parameters is evaluated using a correlation analysis, where the correlation coefficient (CC) between any two parameters is used as an indicator to assess their dependence (or similarity). In general, the value of CC ranges between −1.0 and 1.0, where CC of 1.0 indicates the best correlation in the positive, and CC of −1.0 indicates the best correlation in the negative. A CC value of zero indicates that there is no linear relationship between two parameters. The higher the absolute value of CC, the greater the correlation. If two parameters have stronger relationship based on their CC, one parameter should be eliminated since it can be expressed directly by the other. This research includes considering 11 influencing parameters for compressive strength of GGBS/FA-based GPC, thus contributing to an 11 × 11 CC matrix, as shown in Fig. 4. As described in the figure, all the CC values are in the range of [–0.68, 0.7], except that on the diagonal, which represents self-correlation with the value of one. Generally, if the absolute value of CC is no more than 0.7, only a low correlation exists between two parameters. Consequently, according to the results in the CC matrix, it can be concluded that all 11 influencing parameters can be employed as input variables to design the chemistry-informed surrogate strength prediction model.

4. Development of EBA-optimised chemistry-informed 1D-CNN model

In this section, a novel chemistry-informed surrogate model is

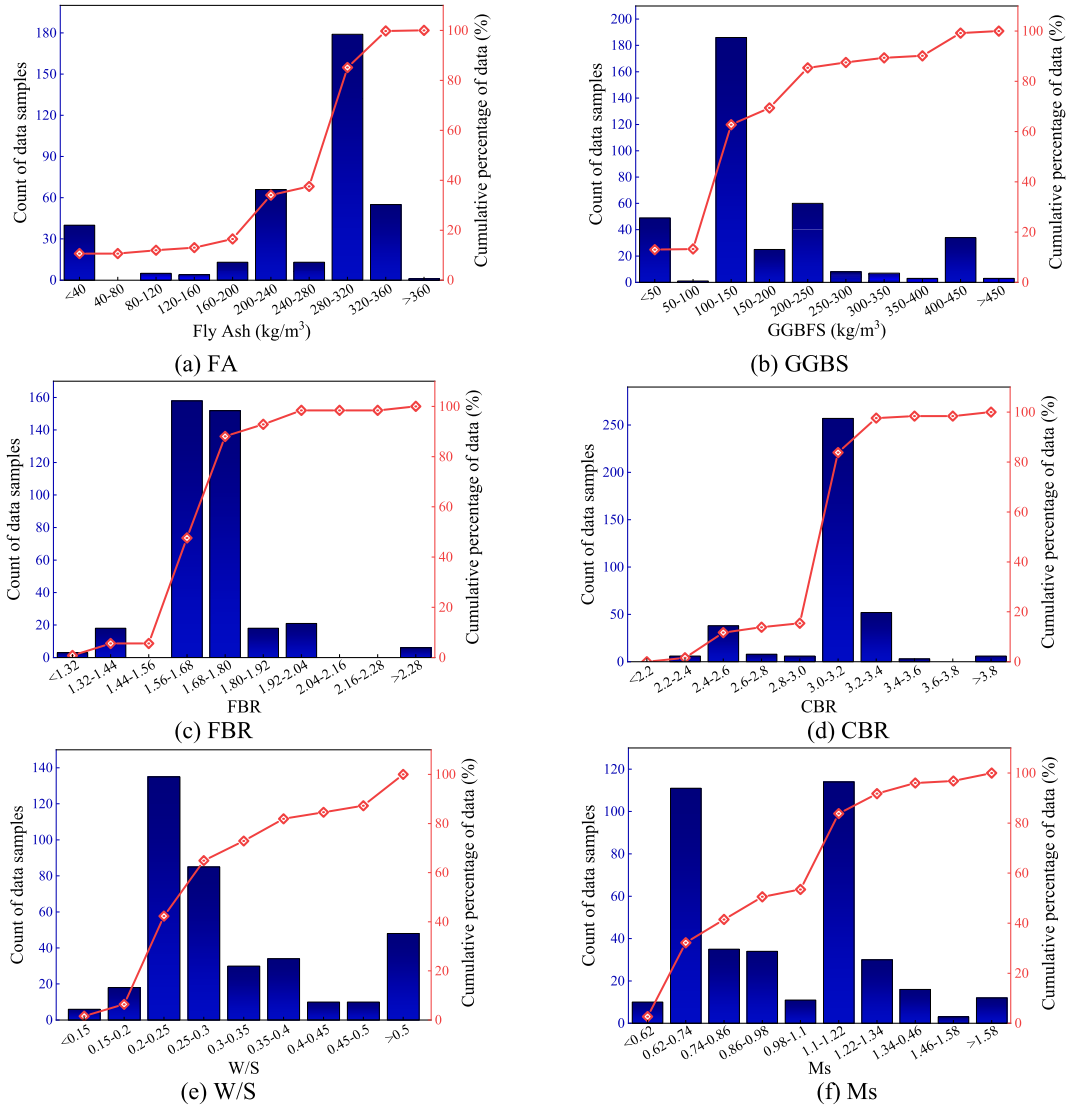

Fig. 3. Frequency distribution analysis of different parameters in this study.

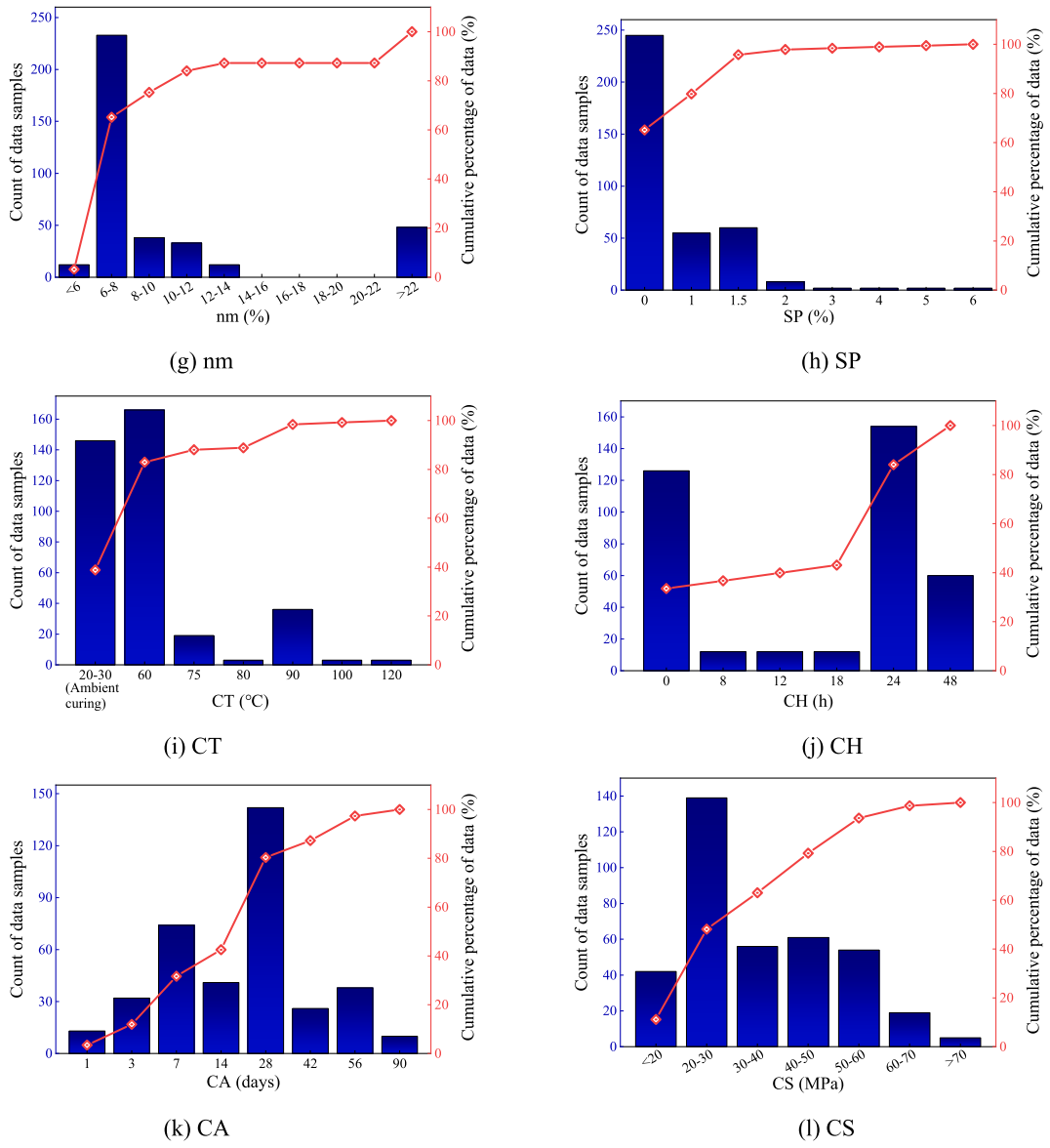

Fig. 3. (*continued*).

developed to predict the compressive strength of GGBS/FA-based GPC, which is based on DL technique. The relevant contents, including model configuration, network training and metaparameter adjustment, are presented in this section.

4.1. Model architecture

The architecture of the proposed 1D-CNN model for strength prediction of GGBS/FA-based GPC is shown in Fig. 5. The whole network is comprised of 1D input layer, convolution layers, pooling layer, FC layers and output layer. The input layer contains 11 neurons, corresponding to 11 influencing factors of strength of GGBS/FA-based GPC, i.e., FA, GGBS, FAG, CAG, W/C, Ms, nm, SP, CT, CH and CA. Following the input layer, the first convolution layer (Conv1), involving several kernels, is added for compressive strength-sensitive feature extraction, where the kernel size is 3×1, the stride is one and the padding is "causal". Then, the second convolution layer (Conv2) is connected to Conv1 for further exploring deep representations, with the kernel size of 3×1, stride of one and causal padding. After two convolution layers, a global max-pooling layer is employed for downsampling learned deep features to contribute a feature map, which is then input into the FC layers. In the proposed model, two FCs, namely FC1 and FC2, with the numbers of neurons in a reducing way, are adopted as the hidden layers for redundant feature elimination and pattern recognition, which outputs the strength of GGBS/FA-based GPC. In the convolution layers, the LReLU is used as the activation function, while the activation function of FC layers is sigmoid function.

Although the input features in this study are not inherently temporal or spatial, the use of 1D-CNN is motivated by its capability to learn and extract local patterns and feature interactions that may not be easily captured by more traditional models such as MLP networks. Additionally, even though the inputs are scalar quantities representing chemical and mix design parameters, their relationships are not strictly independent. The model benefits from the convolutional layer's ability to detect local dependencies and co-variations among groups of features, such as the interplay between chemical activator ratios (Ms and nm) and binder content or water ratios. These interactions, while not sequential in a traditional sense, can still be captured effectively by 1D-CNN filters that scan across input dimensions. Furthermore, weight sharing in CNN kernels reduces overfitting risks with limited training data, where MLP networks are prone to overfitting with dense connections. Accordingly, 1D-CNN offers a balanced approach that captures meaningful feature

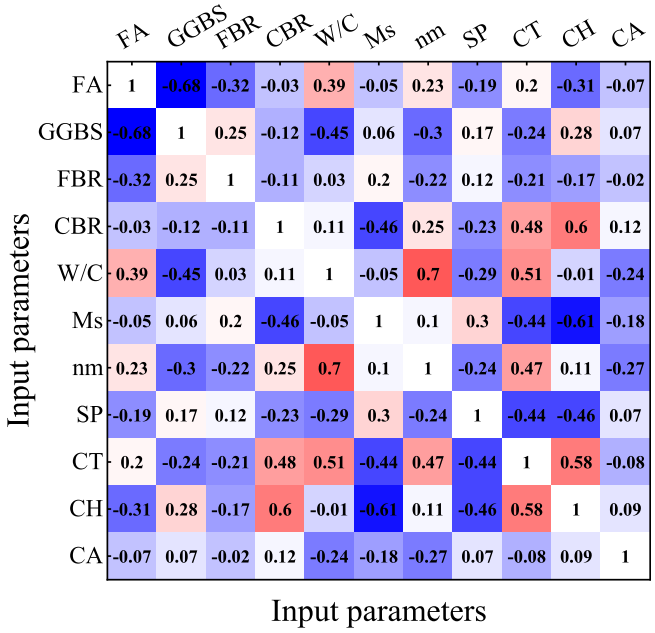

Fig. 4. Correlation coefficient matrix of influencing factors of compressive strength of GGBS/FA-based GPC.

interactions while maintaining generalisation performance, making it a suitable and effective choice for modelling compressive strength of GGBS/FA-based GPC.

4.2. Training of proposed 1D-CNN model

The procedure of 1D-CNN training includes prediction forward propagation and error back-propagation. First, the inputs of influencing factors of compressive strength of GGBS/FA-based GPC are passed through convolution layers, pooling layer, and FC layers to output a prediction value of strength, with initial connection weights and bias of network. Then, the errors between predicted strengths and real values are propagated from output layer back to the input layer reversely. In the back-propagation process, the network weights and biases are continuously updated so that the predicted strength values are close to corresponding real values (Dai et al., 2025; Wang, L. et al., 2024; Yu et al., 2025). This process is repeated until the error reaches a certain threshold, which indicates the network training is finished.

Since the network training is an optimisation procedure on basis of supervised learning, the optimisation objective, i.e., loss function, should be defined to indicate the error between real strength and network predictions. Here, the prediction of compressive strength of GGBS/FA-based GPC can be considered as a regression problem, so the root mean squared error (RMSE) between network outputs and measured strength results is defined as the loss, with the following mathematical expression:

$$Loss(CS, \widehat{CS}) = \sqrt{\frac{1}{N_{ts}} \sum_{k=1}^{N_{ts}} (CS_k - \widehat{CS}_k)^2} \tag{10}$$

where CS_k and $\widehat{CS}_k$ represent kth measured and predicted compressive strength values of GGBS/FA-based GPC, respectively; N_{ts} is the total number of training samples.

In this study, the gradient descent method is adopted to optimise the weights and bias of 1D-CNN model. The forward propagation process of input samples can be formulated as:

$$o^l = fa\left(W^l o^{l-1} + b^l\right) \tag{11}$$

where l denotes the layer number of network; o^l denotes the output of lth layer of network; fa denotes the activation function; W^l and b^l represent the weights and bias of lth layer of network, respectively. Then, the partial derivatives of loss function are calculated to update the connection weights and bias of the network, with the following expressions:

$$W^l = W^l - \alpha \frac{\partial Loss(CS, \widehat{CS})}{\partial W^l} \tag{12}$$

$$b^l = b^l - \alpha \frac{\partial Loss(CS, \widehat{CS})}{\partial b^l} \tag{13}$$

where α denotes the learning rate.

4.3. Metaparameter optimisation of 1D-CNN based on enhanced BA

It is widely known that after the network architecture is confirmed,

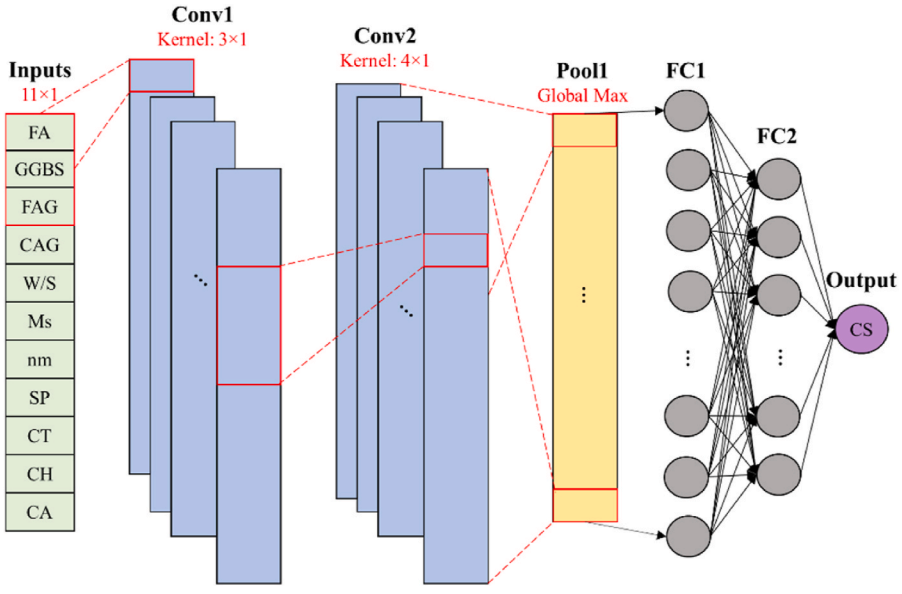

Fig. 5. Architecture of 1D-CNN for compressive strength prediction of GGBS/FA-based GPC.

the generalisation capability of proposed 1D-CNN model is related to the setting of network metaparameters. Metaparameters are the parameters assigned to the 1D-CNN for guiding and controlling the training procedure of network. Different assignments of metaparameters may lead to a wide variety of performance of trained model. Consequently, it is important to optimise the metaparameters of 1D-CNN to achieve the best performance of model in predicting compressive strength of GGBS/FA-based GPC. In this study, the metaparameters of 1D-CNN comprise initial learning rate (η_{ilr}), gradient decay factor (η_{gdf}), L2-regularisation factor (η_{l2r}), learning rate drop period (η_{lrdp}), learning rate drop factor (η_{lrdf}), kernel number of 1st convolution layer (η_{fn1}), kernel number of 2nd convolution layer (η_{fn2}), neuron number of 1st FC layer (η_{fc1}) and neuron number of 2nd FC layer (η_{fc2}). The optimisation target (fitness) is defined as the combination of RMSE and R-squared between real strength results and network predictions in the training process, with the following expression:

$$OT=\frac{\sqrt{\frac{1}{N_{ts}}\sum_{k=1}^{N_{ts}}(CS_k-\widehat{CS}_k)^2}}{\sqrt{\frac{1}{N_{ts}}\sum_{k=1}^{N_{ts}}(CS_k-\widehat{CS}_k)^2}+\left[\frac{N_{ts}\left(\sum_{k=1}^{N_{ts}}CS_k\widehat{CS}_k\right)-\left(\sum_{k=1}^{N_{ts}}CS_k\right)\left(\sum_{k=1}^{N_{ts}}\widehat{CS}_k\right)}{\left[N_{ts}\sum_{k=1}^{N_{ts}}{CS_k}^2-\left(\sum_{k=1}^{N_{ts}}CS_k\right)^2\right]\left[N_{ts}\sum_{k=1}^{N_{ts}}\widehat{CS}_k{}^2-\left(\sum_{k=1}^{N_{ts}}\widehat{CS}_k\right)^2\right]}\right]^2} \tag{14}$$

A lower fitness value indicates a better solution of metaparameters of 1D-CNN. When the fitness approximates zero, the corresponding metaparameters are optimal setting for the model to predict the strength of GGBS/FA-based GPC. Table 3 displays the types and optimisation boundaries of metaparameters of 1D-CNN.

Next, the BA will be used to resolve this optimisation problem for obtaining optimal metaparameters of 1D-CNN model. Despite the fact that BA has been successfully applied in various fields with the benefit of fast convergence, the relevant studies have proven that it suffers from the same shortcomings as other swarm intelligence algorithms, such as insufficient accuracy in finding optimal solution, low efficiency and easy to fall into the local optimum (He et al., 2024; Yuan et al., 2021). The main reason causing these problems is inflexible way of updating velocities and locations of bats. In standard BA, at the beginning of iteration procedure, the slow movement of individual bat may lead to long search time and inefficient convergence, while in the later stage of algorithm search, the accuracy of solution may be significantly affected due to the fast movement of bats.

Aiming for these issues in standard BA, this work proposes an enhanced BA (EBA) for metaparameter optimisation of 1D-CNN model that is developed for compressive strength prediction of GGBS/FA-based GPC, where two significant revisions are introduced. Inspired by the particle swarm optimisation (PSO) algorithm, EBA introduces an adaptive inertia weight coefficient in the formula of velocity update of bats, thus enhancing the local optimisation capability when resolving multi-dimensional complex problems, which is a function of the iteration number. Essentially, in the early stage, the bats are assigned a larger inertia weight coefficient to enhance their exploration ability, leading to better convergence towards optimal solutions. In view of above concerns, this study puts forward a novel adaptive inertia weight coefficient based on hyperbolic tangent function, the expression of which is given by:

$$\tau(it)=\tau_{min}+\frac{(\tau_{max}-\tau_{min})\left(1-\tanh\left(\omega\frac{it}{N_{ts}}-5\right)\right)}{2} \tag{15}$$

where it denotes current iteration number; τ_{min} and τ_{max} denote minimum and maximum inertia weights, respectively; ω is a constant to regulate the diffusion area of curve. Fig. 6 compares the curves of linearly decreased inertia weight and nonlinear decreased inertia weights with different values of ω. It is observed that compared with linear curve, the nonlinear functions can keep a higher inertia weight for a long time initially, and then quickly decline to the minimal value in the later stage of algorithm iteration. This is beneficial for global optimal solution searching of algorithm. As shown in Fig. 6, different values of factor ω will contribute to different shapes of nonlinear curve. In this paper, ω is taken as 10, due to good symmetry of curve, which balances well the exploration and exploitation abilities of bats in different evolution stages.

The second revision is the addition of a random term into the velocity update formula, which aims at boosting the diversity of bat swarm. In the traditional BA, the velocity of individual bat is updated based on the optimal location in the swarm. However, if this optimal location is local optimum rather than global optimum, the algorithm may be trapped in local optimal solution. To address this issue, a random disturbance term is added by considering the location of a randomly selected bat in the swarm to help the algorithm jump out of local optimum. Accordingly, Eq. (5) can be reformulated as:

$$v_i^{t+1}=\tau v_i^t+(x_i^t-x^*)f_i+(x_i^t-x^r)lc \tag{16}$$

where x^r denotes the location of randomly selected bat; lc is the learning factor, the expression of which is given in Eq. (17):

$$lc=lc_{min}+(lc_{max}-lc_{min})\vartheta \tag{17}$$

where lc_{min} and lc_{max} denote the minimum and maximum learning factors, respectively; ϑ is a random number between 0 and 1. On basis of EBA, the metaparameter optimisation procedure of 1D-CNN model for compressive strength prediction of GGBS/FA-based GPC can be divided into the following steps:

1) Determine the algorithm parameters of EBA, including bat population size, solution dimension, initial pulse emission rate, maximum and minimum pulse frequencies, maximum and minimum inertia weights, maximum and minimum learning factors, maximum iteration number, etc.
2) Randomly initialise the individual bats in the swarm.

Table 3
Types and optimisation boundaries of metaparameters.

Name	Type	Range
η_{ilr}	Decimal	[1e-5, 3e-4]
η_{gdf}	Decimal	[0.80, 0.98]
η_{l2r}	Decimal	[1e-10, 1e-2]
η_{lrdp}	Integer	[10, 30]
η_{lrdf}	Decimal	[0.05, 0.30]
η_{fn1}	Integer	[20, 40]
η_{fn2}	Integer	[50, 80]
η_{fc1}	Integer	[30, 50]
η_{fc2}	Integer	[10, 30]

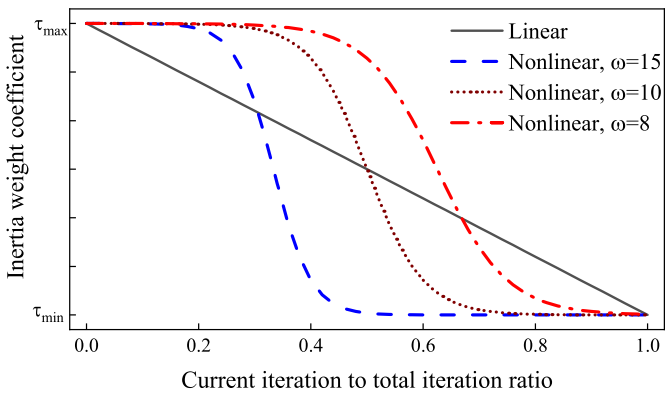

Fig. 6. Comparison of different inertia weight coefficients.

3) Calculate the fitness of each bat, and find out the individual bat with optimal fitness, which is regarded as optimal solution.
4) Utilise Eqs. ((4) and (6) and (15)–(17) to update the velocity and location of each individual bat.
5) Generate a random number $rand_1$ between 0 and 1. If $rand_1 > R_i$, use Eq. (7) to update the current individual bat.
6) Generate a random number $rand_2$ between 0 and 1. If $rand_2 < A_i$ and $OT(x_{new}) > OT(x_{pre})$, use Eqs. (8) and (9) to update the loudness and pulse emission rate.
7) Re-evaluate the fitness of all the bats in the swarm and find out the optimal individual.
8) Judge whether the stopping criterion is satisfied. In this research, the algorithm will be terminated after the current iteration number is more than pre-set maximum number. If so, output the optimal solution; otherwise, go back to 3).

Fig. 7 shows the flowchart of 1D-CNN optimised by EBA for compressive strength prediction of GGBS/FA-based GPC.

4.4. Model performance evaluation metrics

In this study, multiple statistical evaluation metrics are employed to provide a comprehensive assessment of proposed 1D-CNN optimised by EBA for predicting compressive strength of GGBS/FA-based GPC. The metrics include coefficient of determination (R^2), mean absolute error (*MAE*), symmetric mean absolute percentage error (*SMAPE*), mean absolute scaled error (*MASE*), mean directional accuracy (*MDA*) and mean absolute percentage error (*MAPE*). The corresponding mathematical expressions of these indicators are displayed in Eq. (18) to Eq. (22):

$$R^{2=}\left[\frac{N_t\left(\sum_{k=1}^{N_t} CS_k\widehat{CS}_k\right)-\left(\sum_{k=1}^{N_t} CS_k\right)\left(\sum_{k=1}^{N_t}\widehat{CS}_k\right)}{\left[N_t\sum_{k=1}^{N_t} CS_k{}^2-\left(\sum_{k=1}^{N_t} CS_k\right)^2\right]\left[N_t\sum_{k=1}^{N_t}\widehat{CS}_k{}^2-\left(\sum_{k=1}^{N_t}\widehat{CS}_k\right)^2\right]}\right]^2 \tag{18}$$

$$MAE=\frac{\sum_{k=1}^{N_t}|CS_k-\widehat{CS}_k|}{N_t} \tag{19}$$

$$SMAPE=\frac{100\%}{N_t}\sum_{k=1}^{N_t}\frac{|\widehat{CS}_k-CS_k|}{(|\widehat{CS}_k|+|CS_k|)/2} \tag{20}$$

$$MASE=\frac{\frac{1}{N_t}\sum_{k=1}^{N_t}|CS_k-\widehat{CS}_k|}{\frac{1}{N_t-1}\sum_{k=2}^{N_t}|CS_k-CS_{k-1}|} \tag{21}$$

$$MDA=\frac{1}{N_{ts}}\sum_{k=2}^{N_{ts}}1_{sgn(CS_k-CS_{k-1})=sgn(\widehat{CS}_k-CS_{k-1})} \tag{22}$$

where CS_k and $\widehat{CS}_k$ denote kth measured and predicted compressive strength values, respectively; N_t is the number of data samples.

5. Modelling results and discussion

5.1. Model training and test

A predictive model based on 1D-CNN is developed and validated for

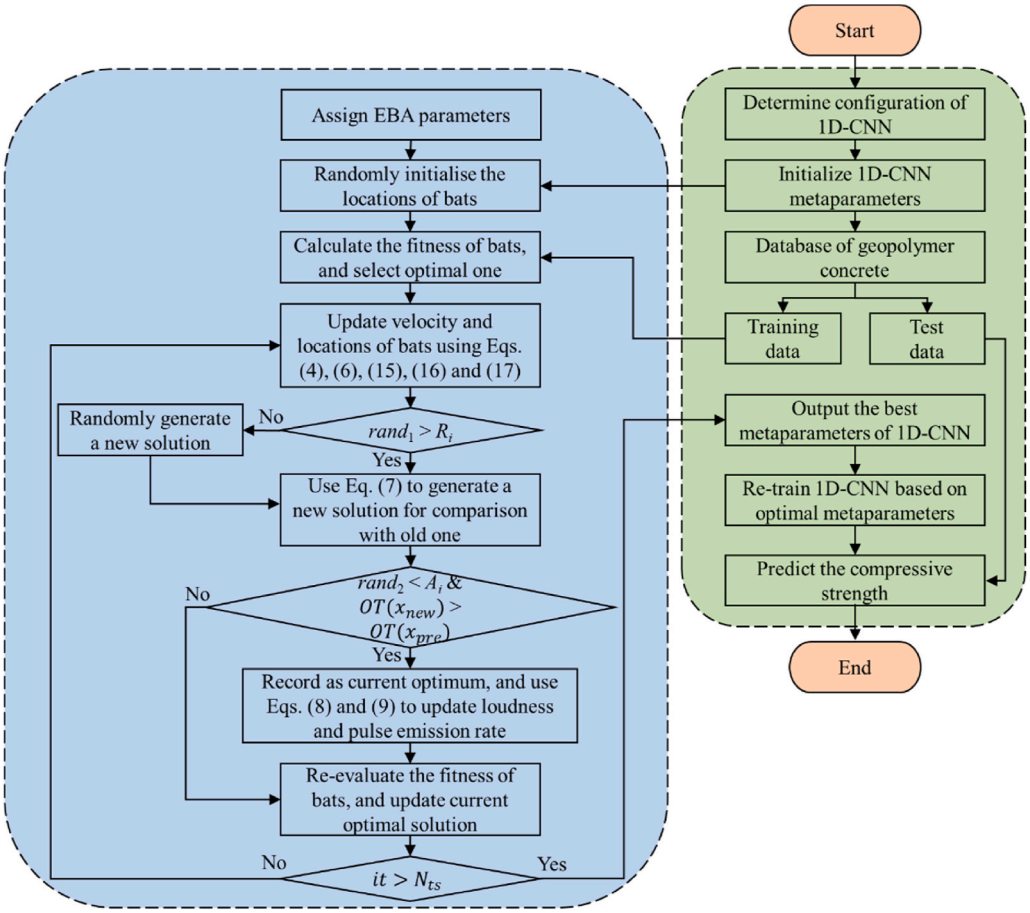

Fig. 7. Schematic of metaparameter optimisation of 1D-CNN for compressive strength prediction.

application of compressive strength evaluation of GGBS/FA-based GPC, using experimental data collected from literature. The dataset is randomly divided into two groups for model training and testing based on the ratio of 7 to 3, in which 70 % of total data samples are used to train the model and the rest 30 % is used as test data for model performance evaluation. The model development and testing based on 1D-CNN and EBA are implemented through Deep Learning Toolbox in MATLAB v.2021b, on a desktop with the configuration of Intel i5-12400F CPU and 16 GB DDR4 RAM. It is well known that meta-parameter optimisation of 1D-CNN using meta-heuristic algorithms is a time-consuming task. To accelerate this process, GPU acceleration is adopted during the training period. The setting of EBA parameters is shown as: bat population size $N = 30$, solution dimension $D = 9$, initial pulse emission rate $R_0 = 0$, maximum pulse frequency $f_{max} = 2.8$, minimum pulse frequency $f_{min} = 1.3$, maximum inertia weight $\tau_{max} = 0.85$, minimum inertia weight $\tau_{min} = 0.15$, maximum learning factor $lc_{max} = 0.6$, minimum learning factor $lc_{min} = 0.3$, loudness and pulse emission rate enhancement coefficients $\alpha = \gamma = 0.9$, and total iteration number $N_{ts} = 200$.

Prior to training the model, all the input variables are standardised

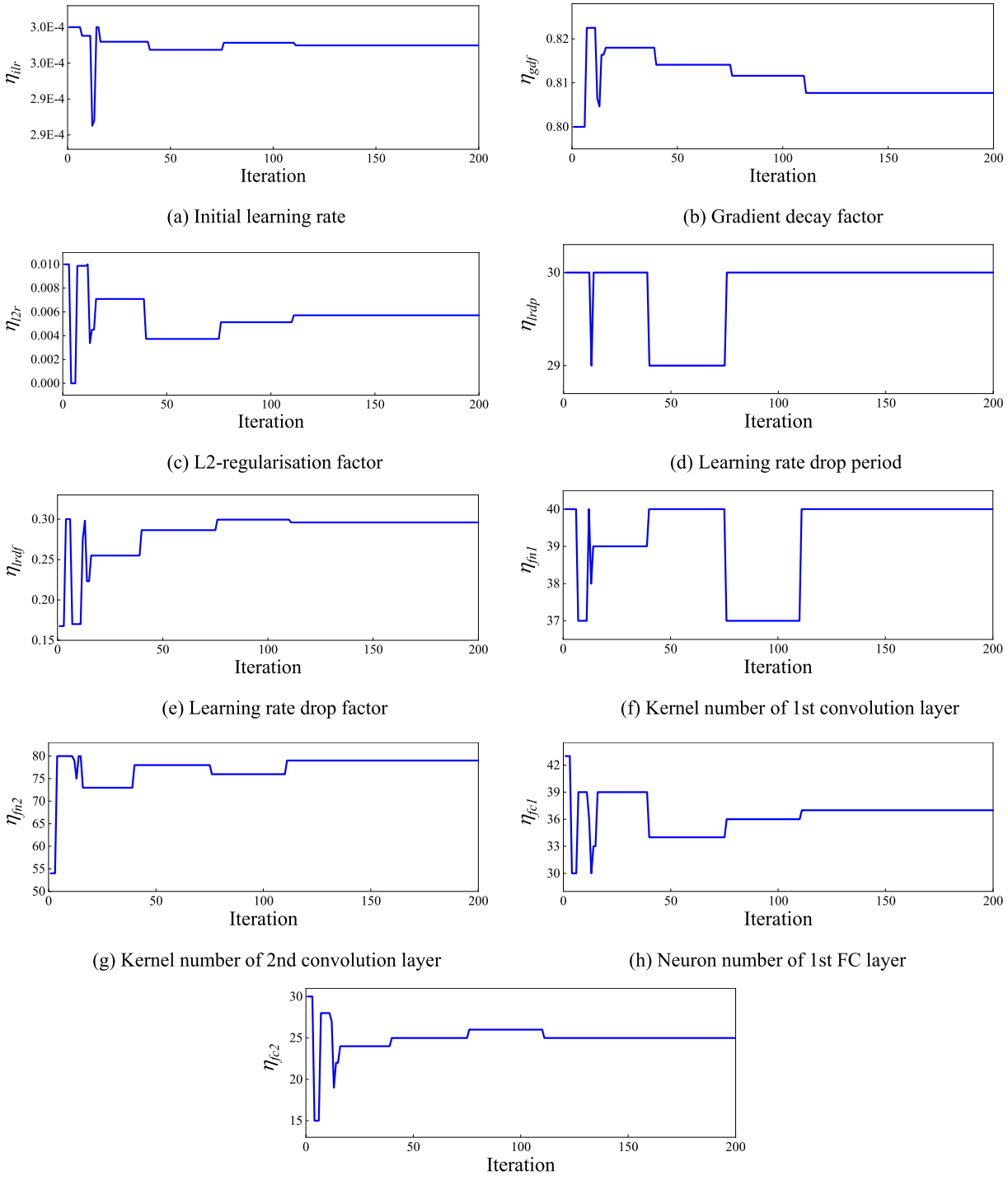

(a) Initial learning rate

(b) Gradient decay factor

(c) L2-regularisation factor

(d) Learning rate drop period

(e) Learning rate drop factor

(f) Kernel number of 1st convolution layer

(g) Kernel number of 2nd convolution layer

(h) Neuron number of 1st FC layer

(i) Neuron number of 2nd FC layer

Fig. 8. Metaparameter optimisation process.

using z-score normalisation. This ensures that all the features contribute comparably during raining and avoids undue influence from features with large numeric ranges (Hu et al., 2025; Zhang et al., 2024). Then, on basis of normalised training data, 1D-CNN model with the architecture in Fig. 5 is established via supervised learning. To avoid potential overfitting during model training, 5-fold cross-validation method is used. Particularly, original training dataset is randomly split into five equally sized subsets. The model then undergoes five rounds of training and validation. In each round, one subset is used as the validation set, while the rest four subsets constitute the training set. By averaging the validation results across all five rounds, this approach provides a more reliable assessment of actual performance of trained model and effectively gauges its ability to generalise to new data. Meanwhile, network metaparameters are tuned for optimal settings by minimising the fitness value in Eq. (14) via an iterative way based on EBA. Fig. 8 shows the iterative optimisation process of nine metaparameters of 1D-CNN for compressive strength prediction of GGBS/FA-based GPC. Apparently, all the metaparameters achieve their optimal values in about 110 iterations, which fully justifies rapid convergence capability of EBA in model parameter optimisation. Table 4 summarises final optimisation results of metaparameters of chemistry-informed 1D-CNN for strength prediction of GGBS/FA-based GPC.

To prove the effectiveness of proposed EBA in metaparameter optimisation of 1D-CNN, an algorithm comparison was undertaken regarding accuracy and convergence. In this investigation, besides the proposed EBA, the standard BA and commonly used PSO with linearly decreasing inertia weight factor (LDIWF-PSO) are included. To make a fair comparison of algorithm performance, the swarm size and total iteration number are set the same for all three algorithms, i.e., 30 and 200, respectively. Other parameters of BA are also the same as that of EBA. For LDIWF-PSO, other parameters are set as: minimum and maximum inertia weight factors are 0.15 and 0.85, respectively, and learning rate is 1.2. Fig. 9 shows the fitness development with increasing iteration of three optimisation algorithms in optimising metaparameters of 1D-CNN for compressive strength prediction of GGBS/FA-based GPC. From the results, it is clearly observed that LDIWF-PSO and BA have faster convergence, but they may be premature because of higher fitness values. The proposed EBA, despite slower convergence, has the lowest fitness due to great local search ability, which makes the algorithm still refine the solution at the later stage of iteration. This outcome sufficiently demonstrates that the proposed EBA outperforms BA and LDIWF-PSO for resolving complex optimisation problem, such as metaparameter optimisation of 1D-CNN, which fully agrees with the findings in Yuan et al. (2021).

Based on the best metaparameters of 1D-CNN, the predictive model is established for compressive strength prediction of GGBS/FA-based GPC. Then, both training and test data were fed into the established chemistry-informed 1D-CNN model for performance assessment. Additionally, to quantify the uncertainty of the proposed predictive model for practical applications, bootstrap resampling is employed to generate prediction intervals by sampling from the model's error distribution. Fig. 10 demonstrates the assessment results in terms of response comparison between experimental results and predicted strength at a 95 % prediction confidence level, where Fig. 10 (a) depicts the results of training data and Fig. 10 (b) corresponds to the results of test data. It is seen that the proposed chemistry-informed 1D-CNN is capable of being accurate in predicting the strength of GGBS/FA-based GPC, with a variety of mix cases and curing conditions. Despite a few outliers, the chemistry-informed 1D-CNN with metaparameter optimisation well traces the tendency of compressive strength. It provides a measure of prediction uncertainty, which is crucial for practical applications where variability in material properties and curing conditions can affect the outcome. Fig. 11 illustrates the prediction errors between experimental values and predicted results for both training and test datasets.

5.2. Performance evaluation

Besides 1D-CNN, several ML techniques have been employed for compressive strength prediction of GPC by scholars over the last few years, with promising results, including SVM (Le et al., 2024), XGBoost (Gad et al., 2024), ANFIS (Wang et al., 2024), and GPR (Singh and Rajhans, 2024). To demonstrate the superiority of proposed method in this research, a comparison study is carried out by comparing chemistry-informed 1D-CNN with EBA-optimised metaparameters to existing predictive models, such as SVM, XGBoost, ANFIS, GPR and 1D-CNN without metaparameter optimisation. The inputs of these ML models are set the same as that of EBA-optimised chemistry-informed 1D-CNN. To ensure a fair comparison, the metaparameters of SVM, XGBoost, ANFIS, and GPR are also optimised during the training phase. The selected metaparameters and corresponding optimisation results are summarised in Table 5. For the baseline 1D-CNN model, the network architecture mirrors that of the proposed model, with the convolution kernel size set to four, the number of kernels set to 40, and the two fully connected layers comprising 40 and 20 neurons, respectively.

To comprehensively evaluate the performance of different ML models and demonstrate the superiority of proposed EBA-optimised chemistry-informed 1D-CNN for compressive strength prediction of GGBS/FA-based GPC, a number of statistical performance assessment indicators are considered in this research, including R^2, *MAE*, *SMAPE*, *MASE*, *MDA* and *MAPE*. The correlation analyses of different models for compressive strength prediction of GGBS/FA-based GPC are presented in Figs.12 to 17, respectively, where Figs. 12–17 (a) indicate the results for training data and Figs. 12–17 (b) correspond to the results for test data. It is observed that for the prediction results of all six models, most data points in the figures are uniformly scattered around the regression line, and only a few data points are out of the boundary lines of ±20%. Among these ML models, the proposed chemistry-informed 1D-CNN optimised by EBA possesses the best capability in strength prediction of GGBS/FA-based GPC, with R^2 of 0.990 and 0.975 for training and test samples, respectively.

Although the ANFIS has a higher R^2 of 0.983 for training data, it performs the worst for the test data, with the lowest R^2 of 0.915, which indicates the overfitting problem of trained model. The CNN has outstanding prediction performance on data with lower strength, but it fails to generate similar accuracy for the GPC with compressive strength less than 40 MPa. The XGBoost and GPR have similar performance on strength prediction, with R^2 of 0.959 and 0.976 for training data, respectively, and 0.930 and 0.931 for test data, respectively. The SVM outperforms ANFIS, GPR, XGBoost and CNN, but is still not as good as the EBA-optimised 1D-CNN regarding R^2 value for both training and test data. Therefore, from the perspective of coefficient of determination, the presented EBA-optimised chemistry-informed 1D-CNN demonstrates the optimal capability in the assessment of strength of GGBS/FA-based GPC.

Fig. 18 presents a comprehensive performance comparison of different models in terms of multiple statistical indicators of *MAE*, *SMAPE*, *MASE*, *MDA* and *MAPE*, via Radar plots, in which the evaluation indicators are calculated on basis of whole dataset. Essentially, higher *MDA* corresponds to the model with better performance. Unlike *MDA*, the lower values of *MAE*, *SMAPE*, *MASE* and *MAPE*, the more accurate

Table 4
Optimal metaparameters of 1D-CNN for compressive strength prediction.

Name	η_{ilr}	η_{gdf}	η_{l2r}	η_{lrdp}	η_{lrdf}	η_{fn1}	η_{fn2}	η_{fc1}	η_{fc2}
Optimum	3E-04	0.808	0.006	30	0.296	40	79	37	25

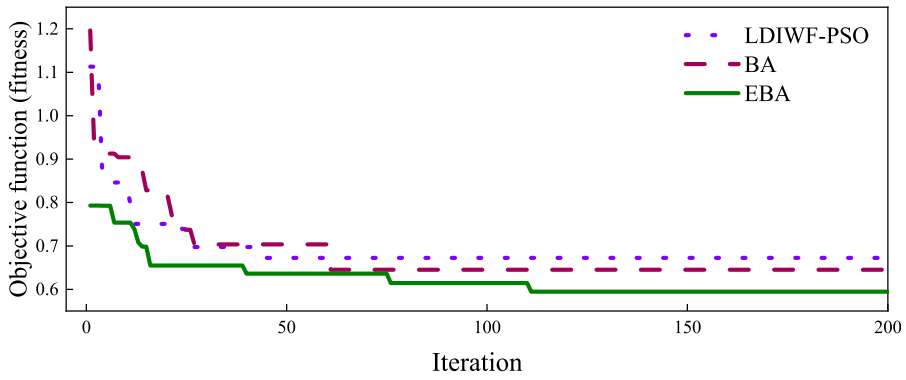

Fig. 9. Comparison of different algorithms for optimising metaparameters of 1D-CNN for compressive strength prediction.

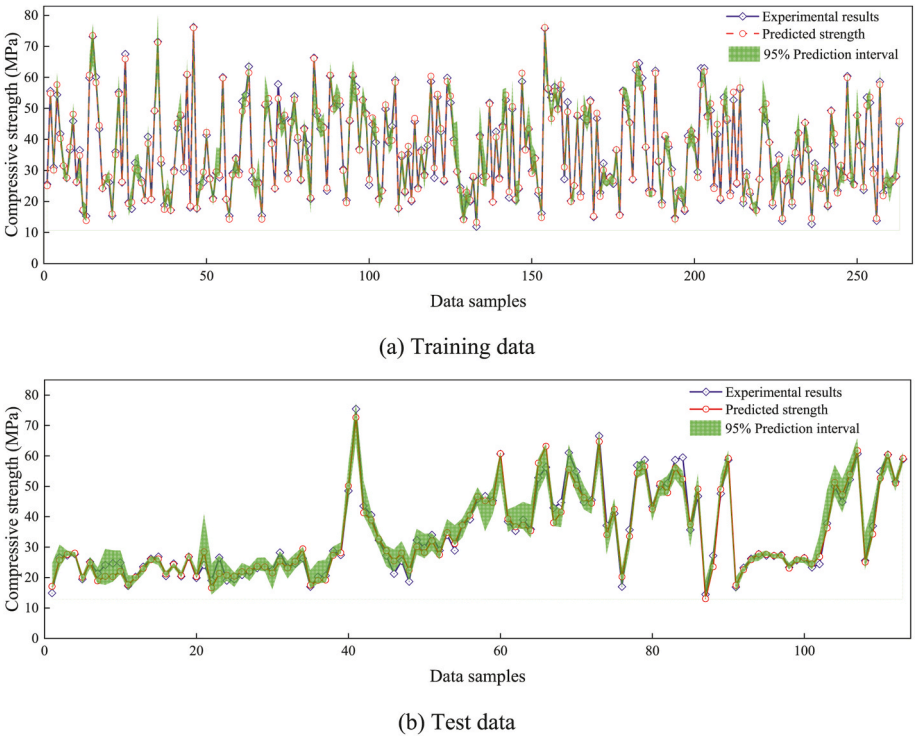

Fig. 10. Sequential comparison of compressive strength between real values and predictions from EBA-optimised chemistry-informed 1D-CNN with 95 % confidence interval.

the evaluated model. By comparison, it is noticeable that proposed EBA-optimised chemistry-informed 1D-CNN has the best assessment indicators of GGBS/FA-based GPC compressive strength prediction among all the models, with the values of *MAE*, *SMAPE*, *MASE*, *MDA* and *MAPE* of 1.23, 0.037, 0.091, 0.952 and 0.038, respectively. The relative errors of five indicators between proposed EBA-optimised chemistry-informed 1D-CNN and other models of XGBoost, SVM, GPR, CNN and ANFIS are 139 %, 15.2 %, 47.1 %, 39.9 % and 49.1 % for *MAE*, 124 %, 17.6 %, 43.9 %, 37.4 % and 64.4 % for *SMAPE*, 140 %, 15.2 %, 47.1 %, 40.0 % and 49.1 % for *MASE*, 3.32 %, 0.25 %, 0.53 %, 0.25 % and 2.48 % for *MDA*, and 125 %, 21.1 %, 46.3 %, 31.7 % and 62.4 % for *MAPE*, respectively. Overall, the chemistry-informed 1D-CNN with metaparameters optimised by EBA has been proven to be the best choice for predicting strength of GGBS/FA-based GPC.

To further verify the superiority of the proposed chemistry-informed 1D-CNN with metaparameters optimised by EBA for modelling the compressive strength of GPC, a comparative study was conducted, focusing on the R^2 and MAE metrics of models from existing studies based on their respective test datasets. In the study by Peng and Unluer (2022), SVM, back-propagation neural network (BPNN), and extreme learning machine (ELM) were used to model compressive strength of FA-based GPC. Gupta and Rao (2022) employed ANN, multiple linear regression (MLR), and multivariate nonlinear regression (MNLR) for 28-day compressive strength prediction of slag/FA-blended GPC. Ahmad et al. (2021) utilised ANN, boosting, and AdaBoost algorithms to evaluate compressive strength of FA-based GPC; Amin et al. (2022) developed models using decision tree (DT), SVM, and random forest (RF) to predict mechanical strength of slag/FA-blended GPC. Nguyen et al. (2024) applied LightGBM, SVM, and cascade forward neural network (CFNN) for strength prediction of slag/fly ash-blended GPC. Abdel-Mongy et al. (2024) used gene expression programming (GEP) and ANN to model compressive strength of slag/FA-blended GPC. The comparison results are presented in Table 6. The proposed model clearly outperformed those from the literature, achieving a higher R^2 of 0.975 and a lower MAE of 1.20 on the test dataset, demonstrating significant improvements in both predictive accuracy and model generalisation. This superior performance can be attributed to the integration of both mix proportions and chemical composition, which allows the model to

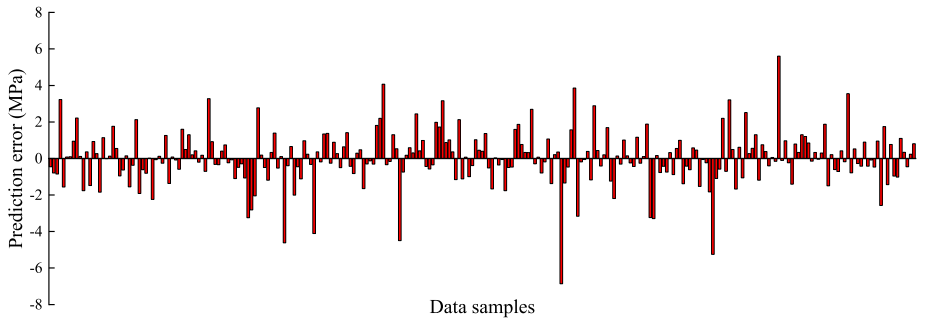

(a) Training data

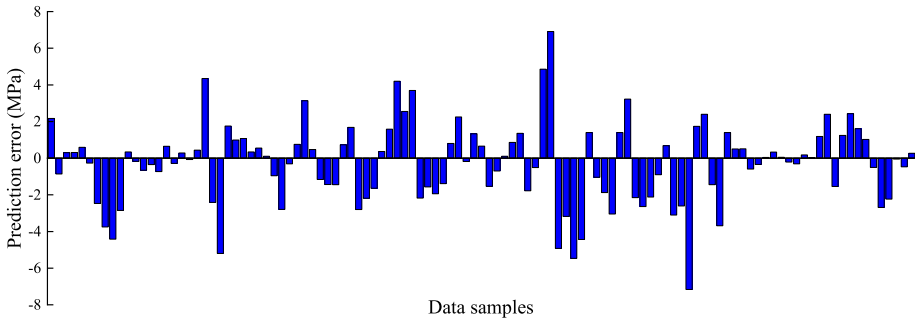

(b) Test data

Fig. 11. Sequential comparison of prediction errors between experimental values and results from EBA-optimised chemistry-informed 1D-CNN.

Table 5
Metaparamters and optimisation results of SVM, GPR, ANFIS, and XGBoost.

Model	Metaparameter	Scale	Optimum
SVM	Box constraint	[0.001, 1000]	0.239
	Kernel scale	[0.001, 1000]	0.862
	Epsilon	[0.001, 1]	0.514
	Kernel function	Gaussian, linear, quadratic, cubic	Gaussian
GPR	Basis function	Constant, zero, linear	Constant
	Kernel function	Isotropic/nonisotropic exponential, Isotropic/ nonisotropic Matern 3/2, Isotropic/nonisotropic Matern 5/2, Isotropic/ nonisotropic rational quadratic, Isotropic/ nonisotropic squared exponential	Nonisotropic squared exponential
	Kernel scale	[0.001, 1000]	0.027
	Sigma	[0.0001, 100]	18.53
ANFIS	No. of membership function	[2, 7]	3
	Membership function type	Triangular, Gaussian, trapezoidal	Gaussian
	Epoch	[10, 1000]	100
XGBoost	Learning rate	[0.001, 0.3]	0.018
	No. of estimators	[50, 2000]	76
	Maximum depth	[3, 12]	6
	Minimum child weight	[1, 10]	1

better capture the complex relationships influencing compressive strength, leading to more accurate predictions than those produced by the other models in the literature.

Fig. 19 displays the Violin plot, which visualises the distributions of absolute deviations between measured compressive strength and predictions from different models by employing hybrid box-plot characteristics and probability density kernel at each end. Compared to conventional box-plot, it explains the complete distribution of dataset. As shown in the figure, the values of Q25 (25 % quartile), Q50 (median) and Q75 (75 % quartile) of different ML/DL models are −0.606, −0.031 and 0.805 for SVM, −3.485, −1.314 and 0.665 for XGBoost, −1.703, 0.008 and 1.643 for ANFIS, −0.703, 0.150 and 0.857 for GPR, −0.940, −0.045 and 0.595 for CNN, and −0.793, 0.023 and 0.764 for proposed EBA-optimised chemistry-informed 1D-CNN, respectively. From the analysis results, it is apparent that the proposed model is more accurate in mimicking the strength of GGBS/FA-based GPC than other models.

5.3. Analysis of model activation function and computational efficiency

To assess the impact of different activation functions on the strength prediction performance of the proposed chemistry-informed 1D-CNN, a comparative study was conducted on four activation functions: Sigmoid, Tanh, ReLU, and LReLU. The study evaluated these functions using metrics of MAE, SMAPE, MASE, MDA, MAPE, and R^2, with the comparison results presented in Fig. 20 as radar plots. It is evident that LReLU outperforms all other activation functions across most evaluation metrics, followed by ReLU, Sigmoid, and Tanh. Specifically, LReLU consistently delivers the best performance, achieving the lowest values of MAE, SMAPE, MASE, and MAPE, indicating superior prediction accuracy. It also performs strongly in MDA and R^2, with the highest values for both, making it the most balanced and effective activation function for predicting the compressive strength of GPC. ReLU follows closely, performing well across all metrics, though slightly trailing behind LReLU. Sigmoid performs better than Tanh but still lags both LReLU and ReLU. Tanh, on the other hand, demonstrates the poorest performance across all metrics, with the highest values for MAE, SMAPE, MASE, and MAPE, and lower values for MDA and R^2. The superior performance of LReLU is attributed to its ability to address the vanishing gradient

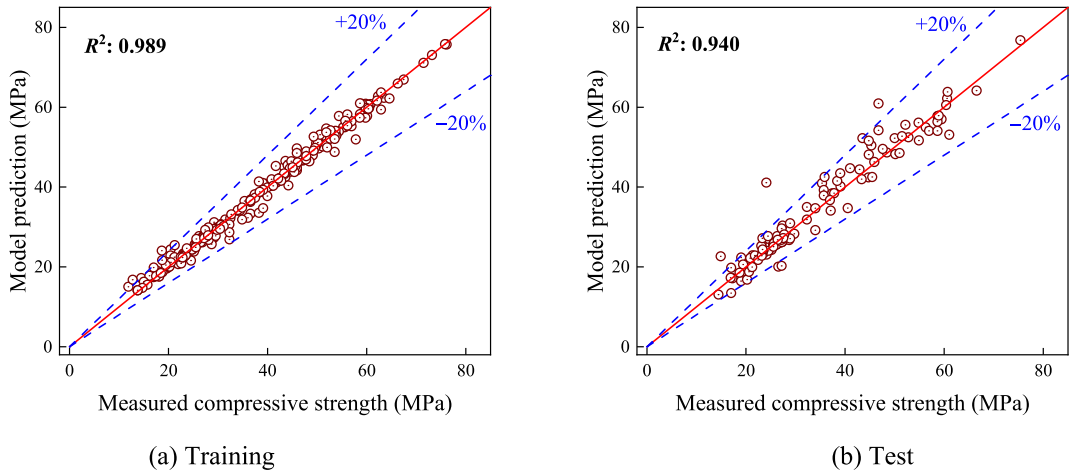

Fig. 12. Regression analysis of SVM for predicting compressive strength of GGBS/FA-based GPC.

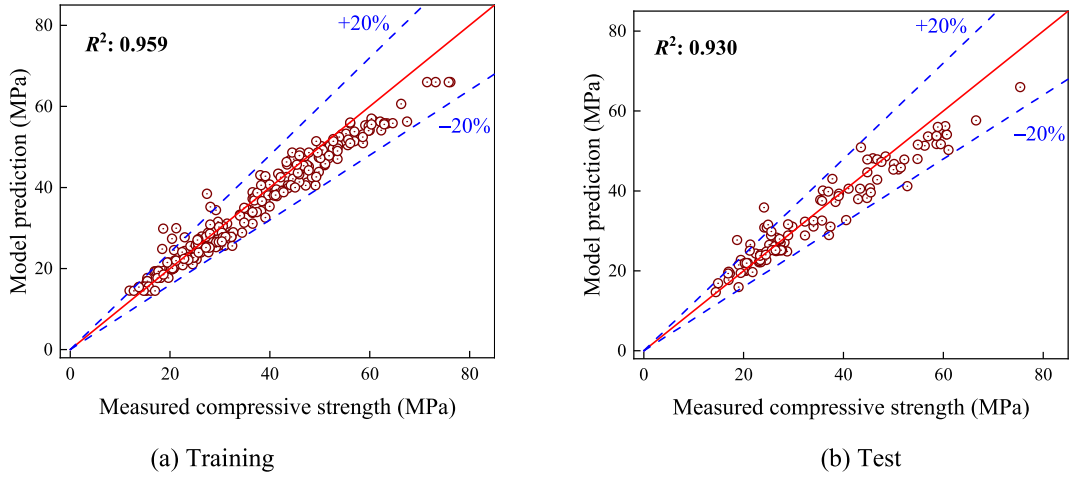

Fig. 13. Regression analysis of XGBoost for predicting compressive strength of GGBS/FA-based GPC.

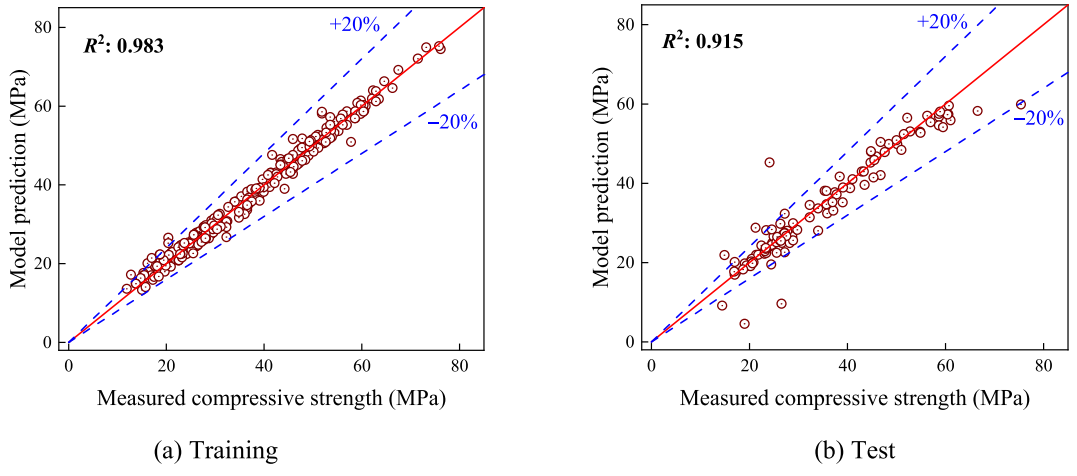

Fig. 14. Regression analysis of ANFIS for predicting compressive strength of GGBS/FA-based GPC.

problem, which affects Sigmoid and Tanh, particularly during back-propagation. LReLU maintains a small, non-zero gradient for negative inputs, preventing neurons from becoming inactive and enhancing the model's training. This characteristic enables LReLU to capture better and propagate relevant information, leading to improved performance across both error and evaluation metrics. Therefore, selecting LReLU as the activation function for the proposed 1D-CNN model is a well-supported choice.

Fig. 21 shows the training and inference times of different models for predicting the compressive strength of GPC. Notably, CNN has the

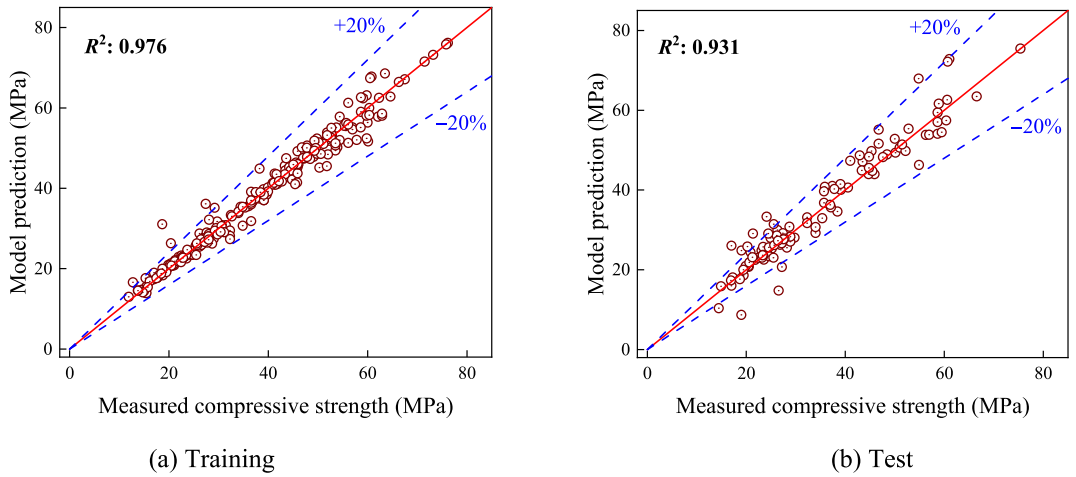

Fig. 15. Regression analysis of GPR for predicting compressive strength of GGBS/FA-based GPC.

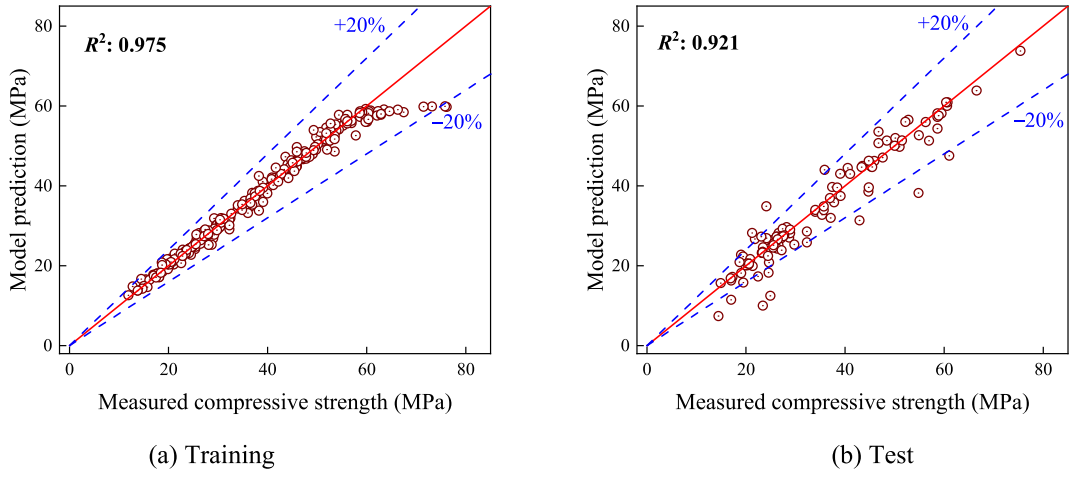

Fig. 16. Regression analysis of CNN for predicting compressive strength of GGBS/FA-based GPC.

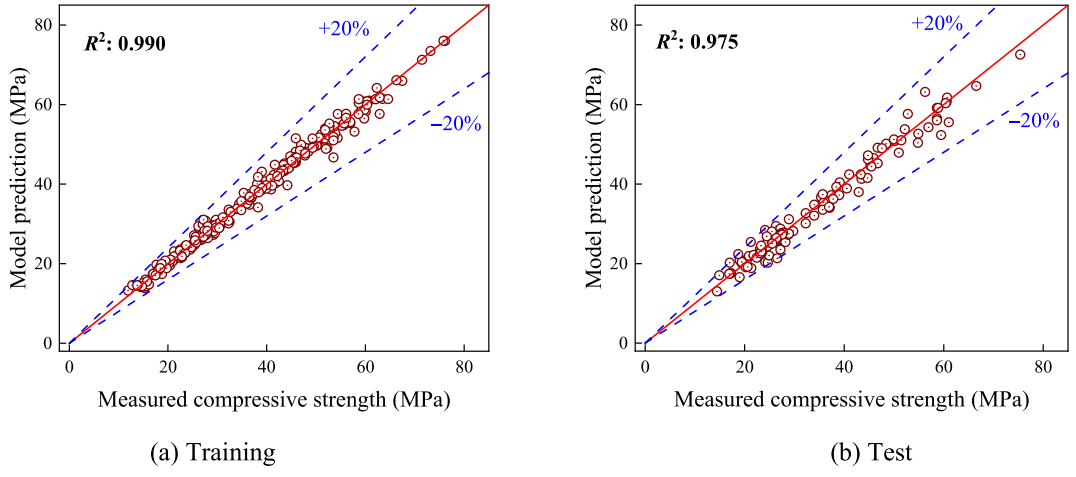

Fig. 17. Regression analysis of proposed model for predicting compressive strength of GGBS/FA-based GPC.

shortest training time due to the lack of metaparameter optimisation, while the other models require longer training times as they optimise the metaparameters. As expected, the proposed model, with a deep network architecture, has the longest training time. This is likely due to the complexity of the deep network, which involves more layers and parameters that require additional computational resources and time to train. However, despite this longer training time, the proposed model stands out with the shortest inference time. This is because the deep architecture of the model, once trained, allows for faster and more efficient processing during inference, benefiting from optimised feature

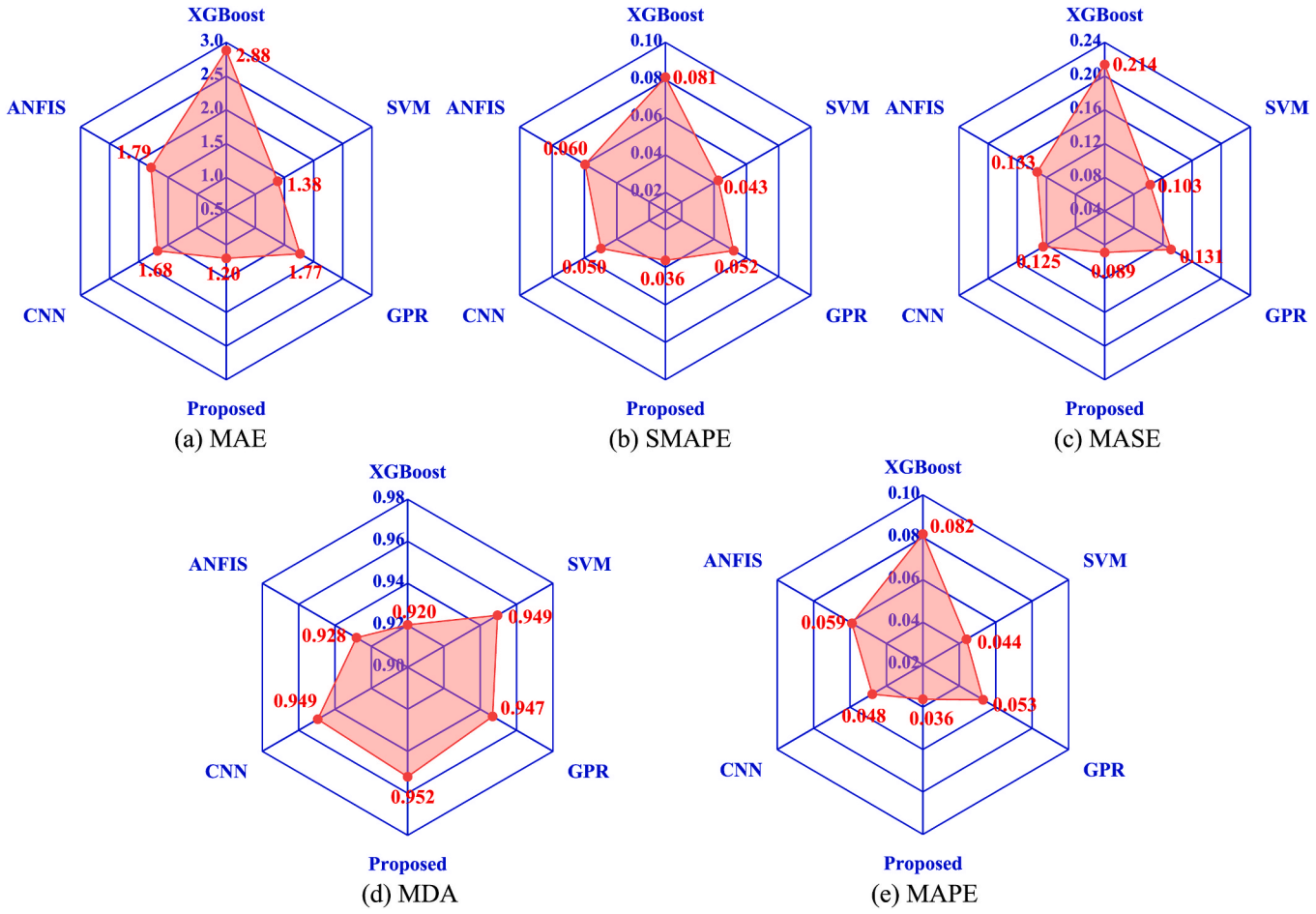

Fig. 18. Radar plots for strength prediction performance comparison of different models.

Table 6
Comparison of proposed model with existing models in the literature for strength prediction of GPC.

Reference	Model	Evaluation metrics	
		R^2	MAE
Peng and Unluer (2022)	SVM	0.956	2.05
	BPNN	0.916	1.59
	ELM	0.904	2.85
Gupta and Rao (2022)	ANN	0.904	1.56
	MLR	0.812	6.11
	MNLR	0.674	5.89
Ahmad et al. (2021)	ANN	0.874	3.86
	Boosting	0.961	1.69
	AdaBoost	0.938	2.16
Amin et al. (2022)	DT	0.921	3.22
	SVM	0.930	3.76
	RF	0.939	3.21
Nguyen et al. (2024)	LightGBM	0.877	3.37
	SVM	0.863	2.89
	CFNN	0.942	3.84
Abdel-Mongy et al. (2024)	GEP	0.656	11.21
	ANN	0.810	5.85
Our study	Proposed	0.975	1.20

extraction and reduced complexity in the prediction phase. In real-world applications, predictive models are typically pre-trained offline and then utilised to evaluate the compressive strength of GPC. Since inference time is a key factor, the proposed chemistry-informed 1D-CNN, with hyperparameters optimised by EBA, offers a significant advantage, making it the preferred choice for the practical application where rapid prediction is crucial.

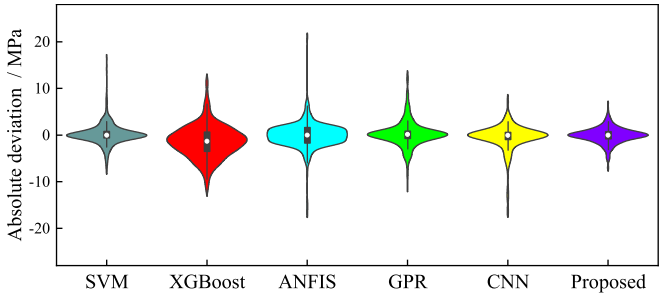

Fig. 19. Violin plot for distribution analysis of absolute deviations of different models.

5.4. Error analysis across input subgroups

To identify potential biases or systematic errors in the model predictions, post hoc analysis is conducted by stratifying the test dataset into subgroups based on key input parameters, such as curing temperature, SP content, and Na_2O-to-binder ratio (nm). For curing temperature, two categories are considered: ambient curing (<30 °C) and oven curing (≥60 °C). Fig. 22(a) shows the distribution of prediction errors for both subgroups. The proposed chemistry-informed 1D-CNN model exhibits slightly higher prediction errors for mixes with ambient curing, where the error distribution is wider, indicating greater variance in predictions. This is likely due to slower geopolymerisation kinetics

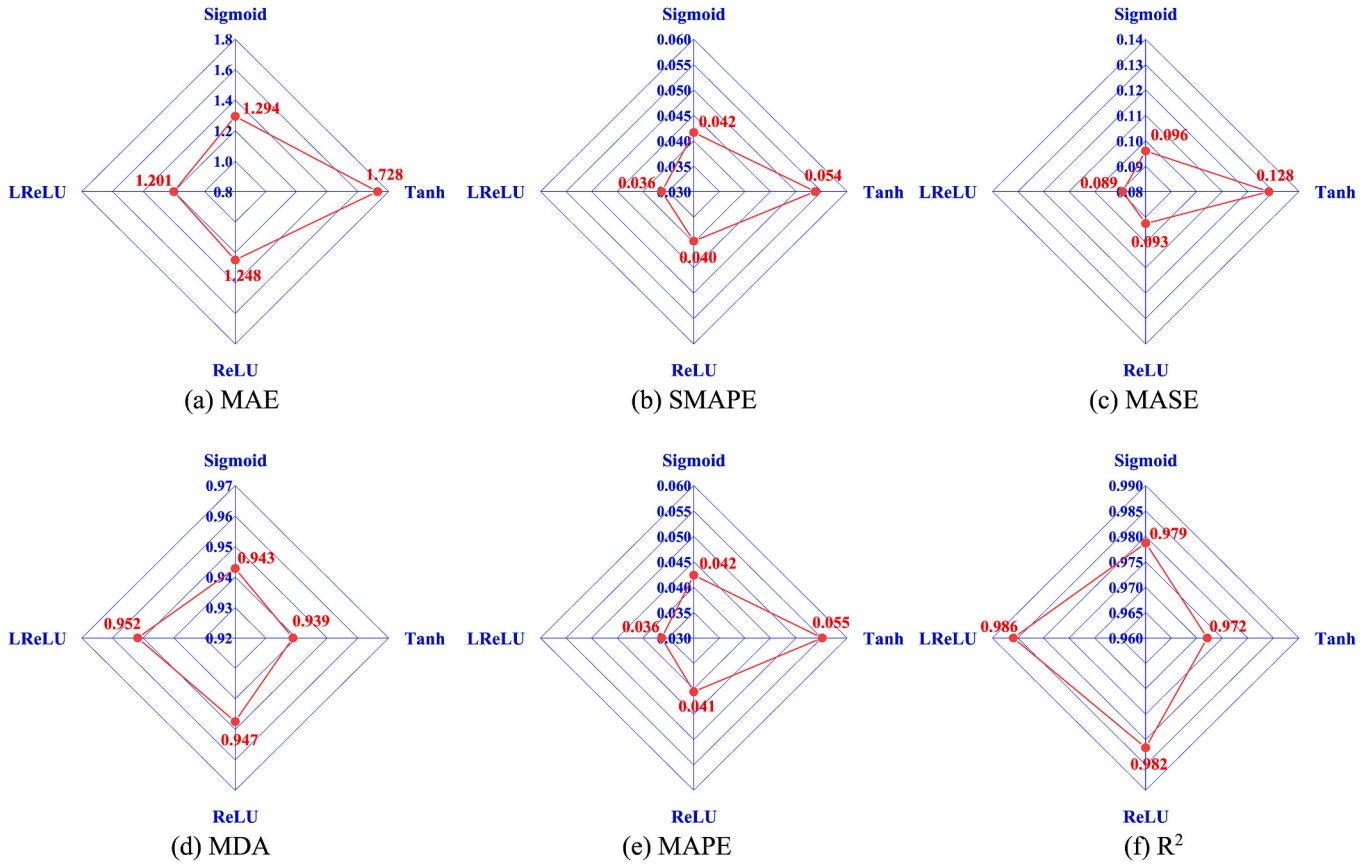

Fig. 20. Radar plots for strength prediction performance evaluation of different activation functions.

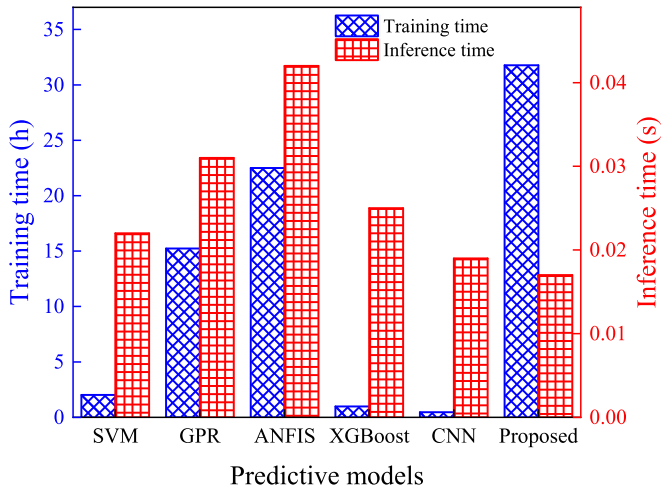

Fig. 21. Training and inference times of different models for compressive strength prediction of GPC.

under ambient conditions, which the proposed model may not fully capture. In contrast, oven-cured samples show a narrower error distribution, indicating that the model performs more consistently when simulating accelerated reactions at higher curing temperature.

For SP content, two subgroups are analysed: those with no SP and those with SP. Fig. 22 (b) shows that mixes containing SP exhibit a wider error distribution, suggesting that the model's predictions are less consistent for these mixes. This may be owing to the nonlinear effect of SP on workability and strength development, which may not be fully captured by the proposed model. On the other hand, mixes without SP show a more concentrated error distribution, indicating better prediction performance in this category.

The Na_2O-to-binder ratio (nm) is also examined by dividing the samples into low (nm<10 %) and high (nm ≥ 10 %) categories. Fig. 22 (c) reveals that the performance of the proposed model is less consistent for samples with high Na_2O-to-binder ratios. The error distribution for these mixes is wider compared to the low Na_2O-to-binder ratio samples, indicating higher prediction errors. This suggests that the model may struggle more with mixes having higher alkali activator dosages, which could introduce complexities in the geopolymerisation process that the proposed model does not fully account for.

5.5. *Model robustness analysis*

In this section, the robustness of proposed chemistry-informed 1D-CNN optimised by EBA for predicting compressive strength of GPC is assessed. Training datasets are randomly selected from the entire dataset, with ratios ranging from 50 % to 90 %, incremented by 10 %. To assess the model's robustness, 100 independent trials are performed for each ratio. During each trial, the model is trained on the selected subset, and its performance is tested using the remaining data. Box plots in Fig. 23 summarise the distribution of six evaluation indicators, including MAR, SMAPE, MASE, MDA, MAPE, and R^2. The results show significant improvement in model performance as the training ratio rises. Indicators such as MAE, SMAPE, MASE, and MAPE decrease, indicating higher accuracy, while MDA and R^2 increase, suggesting better model fit and predictive capability. Notably, the performance gains start to diminish after reaching the training ratio of 70 %, indicating that 70 % offers the optimal balance between performance improvement and computational efficiency. Beyond this point, higher training ratios lead to increase variability in error, as reflected by wider interquartile ranges in the box plots. Therefore, it is reasonable to conclude that the 70 % ratio used in

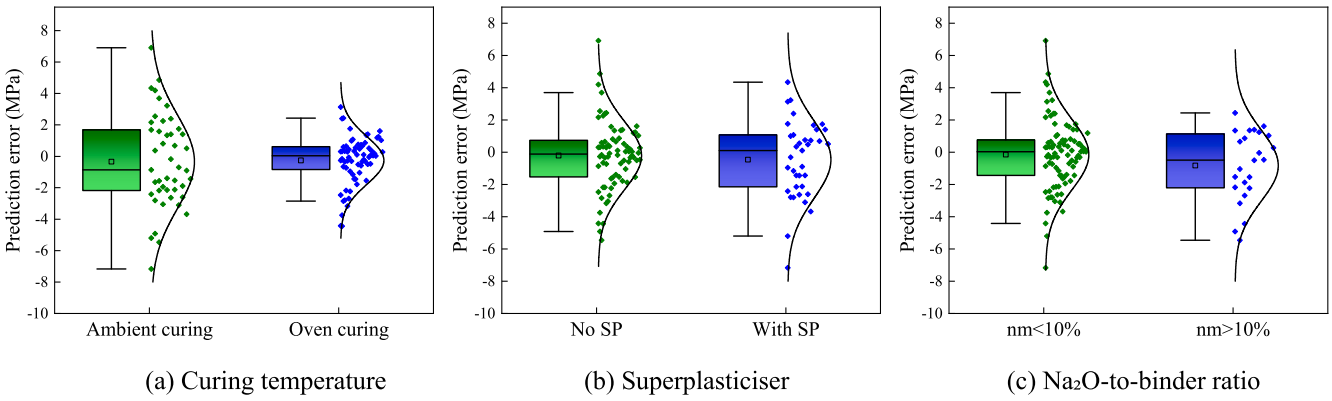

Fig. 22. Post hoc analysis of prediction error patterns for key input variables of proposed model.

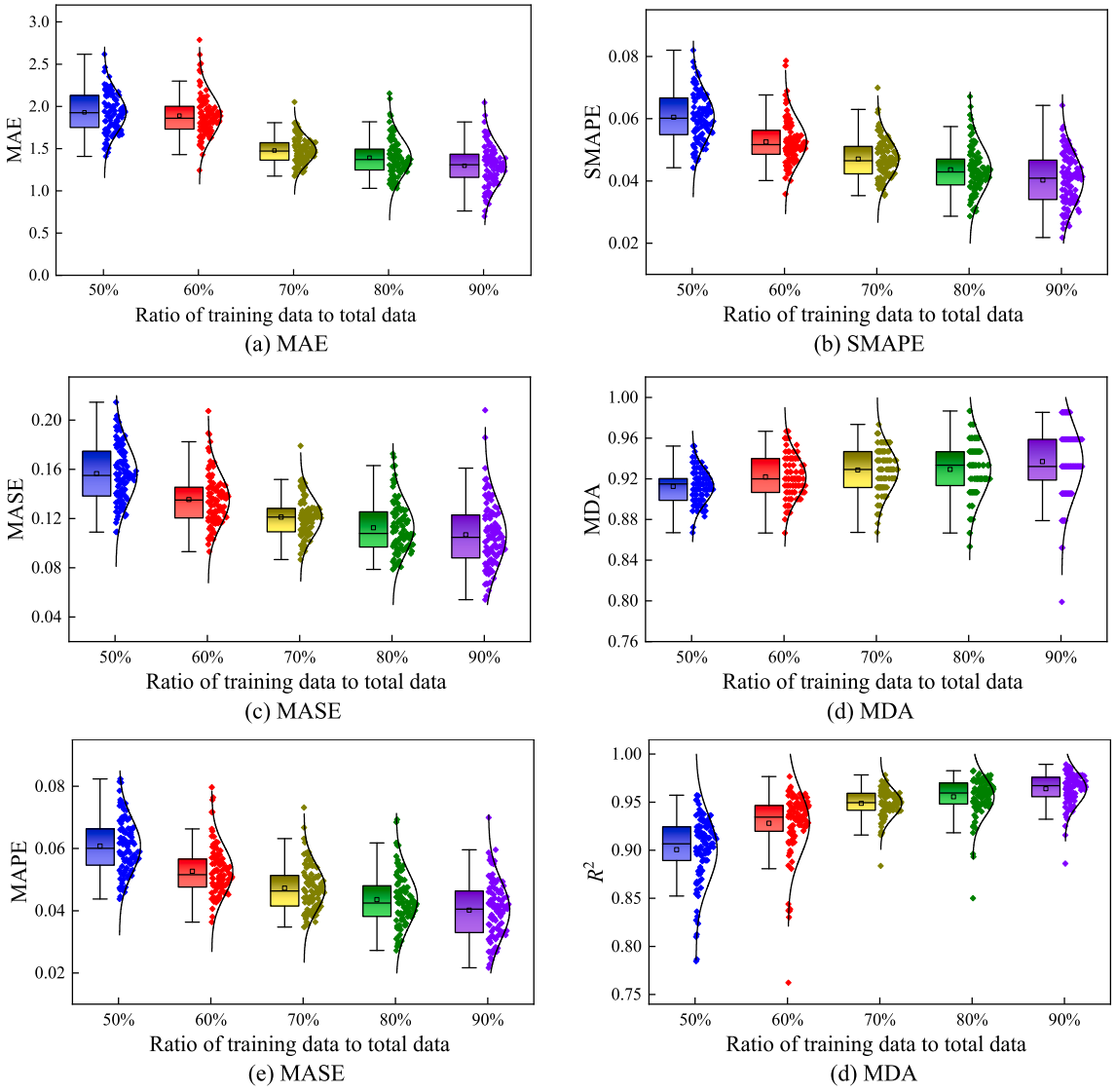

Fig. 23. Distributions of evaluation metrics of proposed model with different ratios of training to total data.

this study strikes a good balance between model accuracy and computational cost. These results highlight the robustness and reliability of the proposed model across varying amounts of training data.

5.6. Interpretation of chemistry-informed EBA optimised 1D-CNN model

Different from conventional empirical models with unambiguous feature representations, the proposed chemistry-informed 1D-CNN model optimised by EBA needs further investigation on the

interpretation of complex and nonlinear relationships between influencing factors and compressive strength of GGBS/FA-based GPC. Hence, model interpretation is undertaken in this section to determine the contribution of each input variable of the proposed model to the strength prediction. Here, SHAP method is employed to interpret the proposed model for strength prediction of GGBS/FA-based GPC. Here, the SHAP values are calculated based on normalised input variables, indicating that they will not affect the ranking of inputs by feature scales. Fig. 24 displays global interpretation by averaging absolute values of SHAP of each model input based on training data. It is evident that nm, W/S, and CA the most significant impact on the model output, with the highest SHAP values over 3. For instance, the study in Yadollahi et al. (2015) also identified the Na_2O to binder ratio as a critical factor, corroborating our results. Following this, CT and Ms also demonstrate considerable influence, though to a slightly lesser extent. GGBS and FA show moderate importance, each contributing notably to the model predictions. CH and FBR are somewhat less influential but still play a role in the model performance. CBR and SP have the smallest SHAP values, indicating that they have the least impact on the model output among the variables considered. Overall, importance ranking of model inputs in Fig. 24 illustrates which variables make the greatest contributions to prediction capability of developed chemistry-informed 1D-CNN optimised by EBA, and how these variables influence compressive strength prediction in the context of a macro-level perspective.

In addition to conducting global interpretation of proposed model, SHAP is also capable of disclosing the dependence of input variables on model output; that is, variation tendency of SHAP value with model inputs, which offers more elaborate understanding of how SHAP values vary with input variables. The corresponding results of all 11 input variables are portrayed in Fig. 25. It is seen that GGBS stands out with a strong positive effect, where SHAP values increase up to 8 as its dosage reaches 400 kg/m^3, confirming its major role in enhancing strength through increased calcium content and C-A-S-H gel formation. Conversely, FA demonstrates a diminishing contribution, with SHAP values declining to −5 at around 300 kg/m^3, indicating that excessive FA may dilute the reactivity. W/S exhibits a steep negative trend, where SHAP values fall from 9 to −10 as the ratio increases from 0.15 to 0.5, emphasising the detrimental effect of excess water on matrix densification and strength. nm demonstrates a strongly positive effect, with SHAP values increasing linearly up to 13 at around 24 of nm, emphasising the crucial role of alkali content in activating the geopolymeric reaction and accelerating strength gain. Ms shows a parabolic trend, with peak SHAP values near 4 at 1.2 of Ms, indicating an optimal activation point beyond which excess alkalinity may reduce workability or cause gel instability. CBR and CH show moderate positive effects, with SHAP values rising to around 5 for 3.5 of CBR and 24 h of CH, suggesting that a balanced coarse aggregate to binder ratio and sufficient early curing duration favor strength gain. FBR presents a wider spread SHAP range from −6 to 8, suggesting a more complex influence that may depend on interactions with other mix proportions. SP, with the SHAP ranging from −3 to 4, shows relatively mild but varied effects, implying that while superplasticiser aids workability, its direct influence on strength is limited. CT shows mixed behavior, but reaches SHAP values as high as 13 around 90 °C, confirming the importance of elevated temperature in accelerating geopolymerisation. CA significantly affects early strength, with SHAP values climbing to 5 by 28 days, then tapering off, indicating that most strength is developed early. In summary, GGBS, nm, W/S ratio, Ms, CT and CA are the most impactful parameters, while FA, SP, and FBR exert more moderate or situational influence on compressive strength.

Additionally, the SHAP-extracted insights are consistent with known experimental results and theoretical perspectives of geopolymer chemistry. For example, the strong positive relationship between nm and compressive strength, evidenced by a SHAP value increase of 13 at higher nm levels, is well-supported by geopolymerisation theory. Alkali concentration plays a critical role in facilitating the dissolution of aluminosilicate precursors and promoting gel nucleation, as described by Davidovits in 2008. These findings are further validated by experimental work from Yadollahi et al. (2015), which demonstrated a 40 % increase in compressive strength when Na_2O content was elevated from 4 % to 10 % in low-calcium geopolymer systems. The parabolic dependency observed for Ms underscores the dual functionality of soluble silicates in geopolymer systems. An optimal Ms ratio ensures a balance between silicate activation and gel polymerisation, whereas excessive SiO_2 content hinders reaction kinetics. This behaviour aligns with research by Firdous and Stephan (2019), who identified an ideal Ms of approximately 1.3 for natural pozzolan-based geopolymers. Beyond this threshold, compressive strength diminishes due to suppressed raw material dissolution and slower reaction rates. The SHAP analysis reinforces the beneficial contribution of GGBS, attributed to its calcium content, which promotes the formation of C-A-S-H gels. Conversely, fly ash exhibits a negative influence at higher dosages exceeding 300 kg/m^3, a trend consistent with its slower reactivity in low-calcium systems under ambient curing conditions, as reported by Castel and Foster (2015) and Nath and Sarker (2014). The dilution effect associated with excessive fly ash incorporation is further corroborated by XRD studies from Hajimohammadi et al. (2019), which revealed a decline in gel phase content when the FA/GGBS ratio surpasses 2. These findings demonstrate that SHAP provides detailed insights into the influence of different variables on strength, making it a powerful tool for exploring the performance boundaries or defining close-ended design solutions.

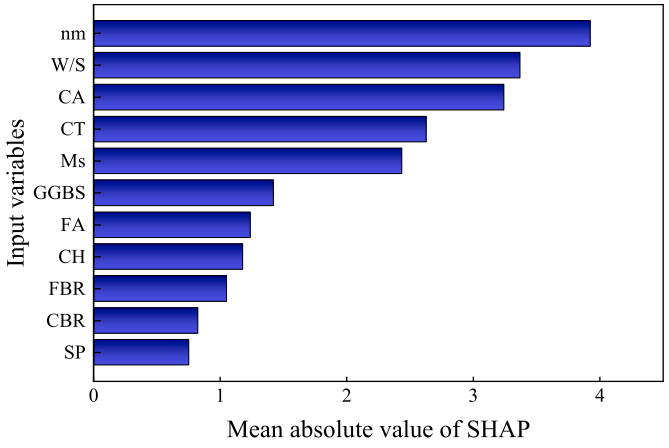

Fig. 24. Global interpretation (importance ranking) of model input variables based on SHAP.

5.7. Assessment of model error and characteristic strength

The model error (*ME*) for the family of products that fit within the boundaries of the test data, and an estimate for the characteristic strength of a desired mix, may be determined by considering the least conservative half of the model predictions plotted against normal inverse probability (z). This is shown in Fig. 26(a) and the model results are demonstrated to be approximately normally distributed. The mean *ME* (i.e., *ME* at z =0) and coefficient of variation (CoV) of the *ME* are 1.013 and 0.072, respectively. For a 75 per cent confidence of a 95 per cent characteristic strength (f_c') based on the applied model, the mean compressive strength (f_{cm}) (as determined from the model) is multiplied by mean(*ME*) x (1–1.75 x CoV). Based on n =113 tests, $f_c' = 0.88 f_{cm}$. Or expressed in terms of mix design, a target mean strength should be taken such that $f_{cm} \geq 1.14 f_c'$. It is worth noting here that other variabilities, such as, for example, due to test machine load cell calibration, sample preparation, curing environment, etc., are directly included in the underpinning data from which the model is derived and, thus, in the model

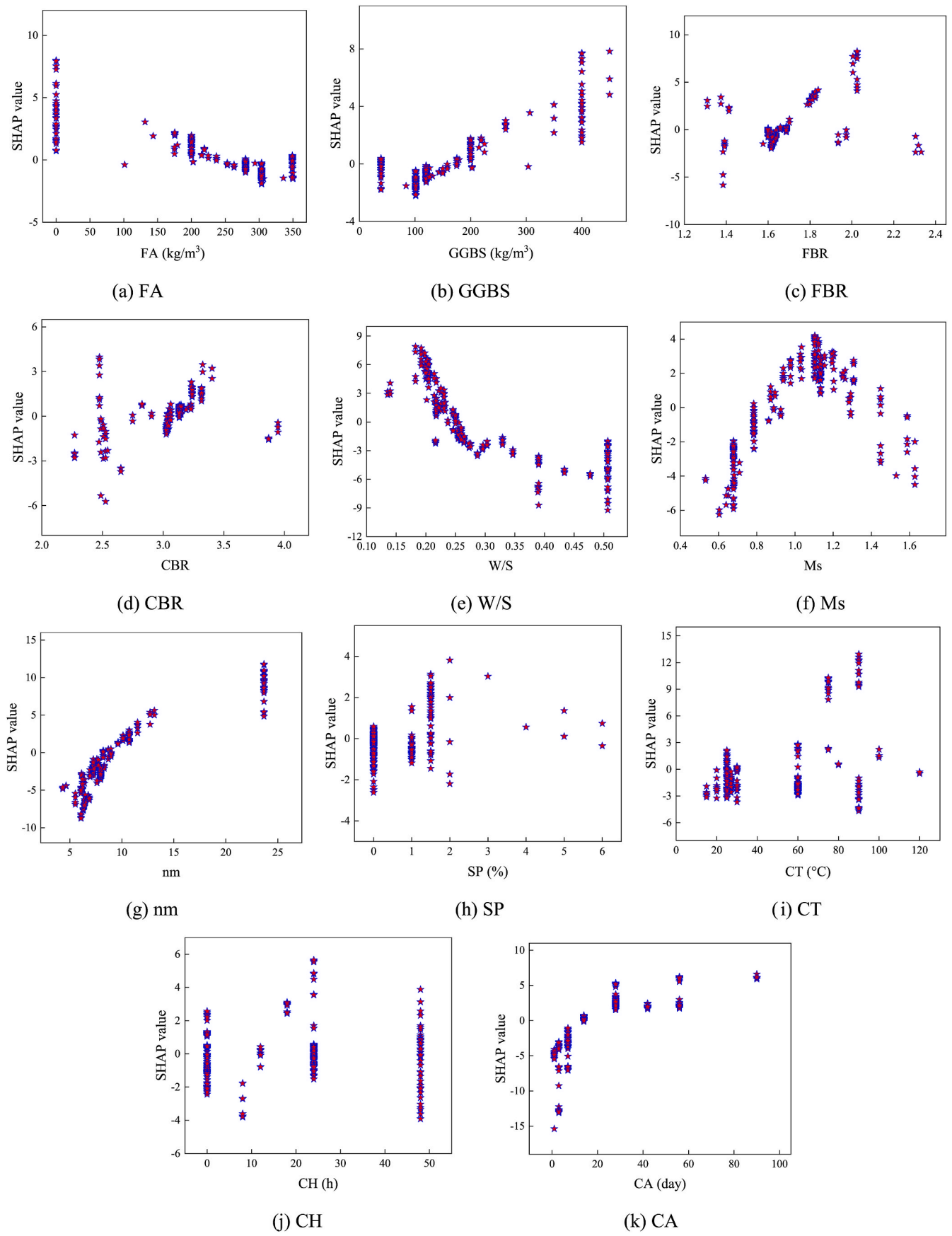

Fig. 25. Dependence analysis of model inputs based on SHAP.

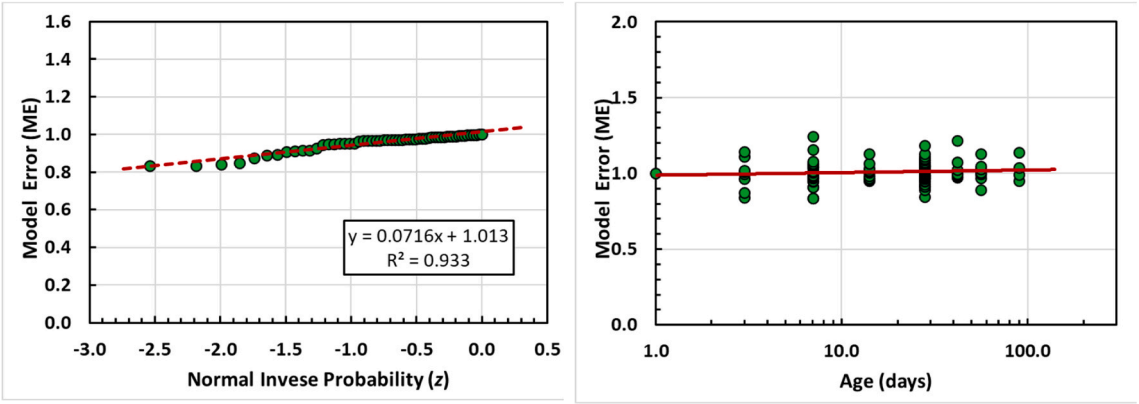

Fig. 26. Model error versus: (a) normal inverse probability; (b) Age in days.

CoV. In Fig. 26(b), the model error is compared to the age of the specimen at the time of testing – it is observed that the results are not biased based on the testing age.

6. Conclusions

GGBS/FA-based GPC is emerging as a promising and eco-friendly alternative to conventional cement-based construction materials. Its advantages lie in the utilisation of industrial waste and low carbon dioxide emission. However, the main obstacle in utilising GPC is ensuring that it possesses the required mechanical properties, particularly in terms of compressive strength. Despite the complexity of the production process, researchers have been working diligently to create a comprehensive formula that considers all the influencing factors that impact mechanical properties of GPC. However, due to many contributing factors, it is challenging to develop such a formula through only experimental means. In this study, a chemistry-informed interpretable model is developed based on 1D-CNN to assess the strength of GGBS/FA-based GPC. To enhance prediction accuracy, the metaparameters of the model were fine-tuned using EBA. The method was trained and evaluated using a comprehensive dataset comprising experimental tests of GGBS/FA-based GPC.

The key findings of the research are:

- The use of EBA results in improved efficiency for optimising metaparameters of 1D-CNN in predicting compressive strength of GGBS/FA-based GPC compared to BA and LDIWF-PSO. This is attributed to its ability to achieve high accuracy and quicker convergence.
- The 1D-CNN model, optimised using EBA, exhibits exceptional results in the determination of compressive strength of GGBS/FA-based GPC. Its performance outstrips that of SVM, XGBoost, ANFIS, GPR and 1D-CNN with pre-defined metaparameters, as evaluated through multiple statistical metrics.
- The SHAP method was employed to analyse the sensitivity of each input variable of EBA optimised 1D-CNN model, which provides both global and local insights into how each input variable influences compressive strength prediction. In the analysis of global level, the results show that nm, CA, W/S and GGBS are the most critical parameters that have a substantial impact on output of surrogate model. In the analysis of local level, the results illustrate that GGBS, nm, SP, CT, CH and CA are the factors that generate positive contributions to strength of GGBS/FA-based GPC, while FA, FBR, CBR and W/S demonstrate negative correlations with model output.
- From analysis of testing data samples using the derived trained model, target mean strengths for a designed mix should not be less than the specified characteristic strength multiplied by a factor of 1.14.
- The chemistry-informed approach transforms SHAP outputs from statistical indicators to actionable materials science insights. Users gain direct guidance on alkali-activation tuning, GGBS/FA balancing, and curing optimisation, reducing trial-and-error in mix design.

Although the chemistry-informed 1D-CNN model optimised by EBA shows promising results, its performance depends on the quality and representativeness of the dataset, which may not capture all real-world variations. The model's generalisation is also limited by a fixed set of input variables, and further optimisation may be needed as new parameters emerge. In addition to this, the model requires significant computational resources for training, especially during metaparameter tuning. Although SHAP values improve interpretability, the model's complexity may still pose challenges in providing simple, actionable insights for mix design.

To address these issues, future research should focus on expanding the dataset to include a wider range of material sources, testing conditions, and mix designs to improve the model's generalisation. Incorporating additional relevant variables or exploring more flexible input features could further enhance the model's robustness. Additionally, future work will look into incorporating more detailed material characterisation, such as fineness and specific amorphous content, where consistently available. Data augmentation approaches, such as the synthetic minority oversampling technique (SMOTE) and adversarial generative networks (GAN), will be employed to generate artificial data in future work. These techniques are expected to enhance model generalisability and improve the prediction accuracy of compressive strength for GGBS/FA-based GPC, especially for under-represented mix designs. Further optimisation of the model may also involve the development of more efficient training algorithms to reduce computational demand. Moreover, increasing the interpretability of the model through simpler or more intuitive methods could make it more accessible for practical applications in mix design. Finally, integrating real-time data and adaptive transfer learning techniques could allow the model to continuously improve and stay relevant across varying material compositions and curing conditions.

On the other hand, the proposed model in this research can be adapted for other aluminosilicate systems, such as binders containing metakaolin or biomass ash. However, challenges may arise in terms of the input parameter space and model design. The primary challenge is the variability in chemical composition and reactivity among different aluminosilicate sources. For instance, metakaolin and biomass ash may exhibit different alumina and silica content compared to fly ash and GGBS, leading to variations in geopolymerisation kinetics and compressive strength development. To address this challenge, additional data specific to metakaolin or biomass ash-based geopolymers

will be incorporated in future work to extend the model's applicability to these alternative binder systems. Furthermore, domain adaptation transfer learning technique will be employed to adapt the model, leveraging knowledge from a source domain, such as GGBS/FA-based GPC, and transferring it to a target domain, such as metakaolin or biomass ash-based GPC, with minimal data. However, a key issue in domain adaptation is the potential feature discrepancy between the source and target domains. These discrepancies may arise due to differences in the chemical composition, curing conditions, or other material characteristics between the source and target systems. To mitigate this problem of feature discrepancies, in future work, we will add a discrepancy term to the loss function of the proposed 1D-CNN model. This term would explicitly penalise the model for mismatches in the feature distributions between the source and target domains, encouraging the model to learn domain-invariant features. Methods such as maximum mean discrepancy (MMD) or adversarial domain adaptation could be incorporated into the loss function, allowing the model to align better the feature spaces of the source and target domains. By incorporating domain adaptation transfer learning technique, the model can better generalise across different binder systems and improve prediction accuracy for other aluminosilicate systems.

Lastly, future research should experimentally validate SHAP-derived insights by systematically testing mixtures designed with critical values of nm or Ms as identified by the proposed model. Controlled experiments could confirm whether these thresholds indeed correspond to optimal performance. Additionally, incorporating advanced material characterisation techniques such as nuclear magnetic resonance spectroscopy and X-ray diffraction would help clarify the underlying chemical mechanisms and resolve any remaining ambiguities in reaction pathways.

CRediT authorship contribution statement

Yang Yu: Writing – original draft, Resources, Methodology, Conceptualization. **Iman Munadhil Abbas Al-Damad:** Writing – review & editing, Data curation. **Stephen Foster:** Writing – review & editing, Project administration, Funding acquisition, Formal analysis. **Ali Akbar Nezhad:** Writing – review & editing, Funding acquisition. **Ailar Hajimohammadi:** Writing – review & editing, Supervision, Funding acquisition.

Declaration of competing interest

The authors declare that they have no known competing financial interests or personal relationships that could have appeared to influence the work reported in this paper.

Acknowledgement

This research is supported by Australian Research Council (Grant No. LP200100531) and industry partner Boral. The authors would like to acknowledge both technical and financial support from the funding bodies.

Appendix A. Supplementary data

Supplementary data to this article can be found online at https://doi.org/10.1016/j.dibe.2025.100736.

Data availability

Data will be made available on request.

References

Abdel-Mongy, M., Iqbal, M., Farag, M., Yosri, A., Alsharari, F., Yousef, S.E.A., 2024. Artificial intelligence prediction of one-Part Geopolymer compressive strength for sustainable concrete. CMES-Comp. Mod. Eng.,Sci. 141 (1).
Adewumi, A.A., Mohd Ariffin, M.A., Maslehuddin, M., Yusuf, M.O., Ismail, M., Al-Sodani, K.A.A., 2021. Influence of silica modulus and curing temperature on the strength of alkali-activated volcanic ash and limestone powder mortar. Materials 14 (18), 5204.
Ahmad, A., Ahmad, W., Aslam, F., Joyklad, P., 2022. Compressive strength prediction of fly ash-based geopolymer concrete via advanced machine learning techniques. Case Stud. Constr. Mater. 16, e00840.
Ahmad, A., Ahmad, W., Chaiyasarn, K., Ostrowski, K.A., Aslam, F., Zajdel, P., Joyklad, P., 2021. Prediction of geopolymer concrete compressive strength using novel machine learning algorithms. Polymers 13 (19), 3389.
Ai, L., Bayat, M., Ziehl, P., 2023. Localizing damage on stainless steel structures using acoustic emission signals and weighted ensemble regression-based convolutional neural network. Measurement 211, 112659.
Ai, L., Soltangharaei, V., Ziehl, P., 2022. Developing a heterogeneous ensemble learning framework to evaluate Alkali-silica reaction damage in concrete using acoustic emission signals. Mech. Syst. Signal Process. 172, 108981.
Allahverdi, A., Kani, E.N., Esmaeilpoor, S., 2008. Effects of silica modulus and alkali concentration on activation of blast-furnace slag. Iranian J. Mate. Sci. Eng. 5 (2), 32–35.
Alyami, M., Khan, M., Javed, M.F., Ali, M., Alabduljabbar, H., Najeh, T., Gamil, Y., 2024. Application of metaheuristic optimization algorithms in predicting the compressive strength of 3D-printed fiber-reinforced concrete. Devel. Built Environ. 17, 100307.
Amin, M., Elsakhawy, Y., Abu el-hassan, K., Abdelsalam, B.A., 2022a. Behavior evaluation of sustainable high strength geopolymer concrete based on fly ash, metakaolin, and slag. Case Stud. Constr. Mater. 16, e00976.
Amin, M.N., Khan, K., Javed, M.F., Aslam, F., Qadir, M.G., Faraz, M.I., 2022b. Prediction of mechanical properties of fly-ash/slag-based geopolymer concrete using ensemble and non-ensemble machine-learning techniques. Materials 15 (10), 3478.
Awoyera, P.O., Kirgiz, M.S., Viloria, A., Ovallos-Gazabon, D., 2020. Estimating strength properties of geopolymer self-compacting concrete using machine learning techniques. J. Mater. Res. Technol. 9 (4), 9016–9028.
Bahmani, H., Mostofinejad, D., Eftekhar, M.R., 2024. A novel eco-friendly thermal-insulating high-performance geopolymer concrete containing calcium oxide-activated materials with waste tire and waste polyethylene terephthalate. Devel. Built Environ. 18, 100473.
Bakharev, T., 2005. Geopolymeric materials prepared using Class F fly ash and elevated temperature curing. Cement Concr. Res. 35 (6), 1224–1232.
Castel, A., Foster, S.J., 2015. Bond strength between blended slag and Class F fly ash geopolymer concrete with steel reinforcement. Cement Concr. Res. 72, 48–53.
Chithambaram, S.J., Kumar, S., Prasad, M.M., Adak, D., 2018. Effect of parameters on the compressive strength of fly ash based geopolymer concrete. Struct. Concr. 19 (4), 1202–1209.
Cong, X., Zhou, W., Elchalakani, M., 2020. Experimental study on the engineering properties of alkali-activated GGBFS/FA concrete and constitutive models for performance prediction. Constr. Build. Mater. 240, 117977.
Dai, L., Wu, P., Yang, H., Lee, D., Zhang, W., Wang, L., 2025. Practical model for flexural capacity of corroded PC structures based on interpretable machine learning. Adv. Struct. Eng. 28 (8), 1403–1417.
Das, S.K., Shrivastava, S., 2021. Siliceous fly ash and blast furnace slag based geopolymer concrete under ambient temperature curing condition. Struct. Concr. 22, E341–E351.
Davidovits, J., 2008. Geopolymer Chemistry and Applications. Geopolymer Institute.
De Larrard, F., 1999. Concrete Mixture Proportioning: a Scientific Approach. CRC Press.
de Larrard, F., Colina, H., 2019. Concrete Recycling: Research and Practice. CRC Press.
Deb, P.S., Nath, P., Sarker, P.K., 2014. The effects of ground granulated blast-furnace slag blending with fly ash and activator content on the workability and strength properties of geopolymer concrete cured at ambient temperature. Mater. Des. 62, 32–39.
Deb, P.S., Nath, P., Sarker, P.K., 2015. Drying shrinkage of slag blended fly ash geopolymer concrete cured at room temperature. Procedia Eng. 125, 594–600.
Deng, F., He, Y., Zhou, S., Yu, Y., Cheng, H., Wu, X., 2018. Compressive strength prediction of recycled concrete based on deep learning. Constr. Build. Mater. 175, 562–569.
Dunphy, K., Sadhu, A., Wang, J., 2022. Multiclass damage detection in concrete structures using a transfer learning-based generative adversarial networks. Struct. Control Health Monit. 29 (11), e3079.
Duxson, P., Fernández-Jiménez, A., Provis, J.L., Lukey, G.C., Palomo, A., van Deventer, J. S., 2007. Geopolymer technology: the current state of the art. J. Mater. Sci. 42, 2917–2933.
Fang, G., Ho, W.K., Tu, W., Zhang, M., 2018. Workability and mechanical properties of alkali-activated fly ash-slag concrete cured at ambient temperature. Constr. Build. Mater. 172, 476–487.
Fernández-Jiménez, A., Palomo, A., 2003. Characterisation of fly ashes. Potential reactivity as alkaline cements. Fuel 82 (18), 2259–2265.
Firdous, R., Stephan, D., 2019. Effect of silica modulus on the geopolymerization activity of natural pozzolans. Constr. Build. Mater. 219, 31–43.
Gad, M.A., Nikbakht, E., Ragab, M.G., 2024. Predicting the compressive strength of engineered geopolymer composites using automated machine learning. Constr. Build. Mater. 442, 137509.

Gao, H., Al-Damad, I.M.A., Siddika, A., Kim, T., Foster, S., Hajimohammadi, A., 2025a. Enhancing the workability retention of one-part alkali activated binders by adjusting the chemistry of the activators. Cem. Concr. Compos. 157, 105928.
Gao, H., Hamed, E., Al-Damad, I.M.A., Hajimohammadi, A., Foster, S., 2025b. Creep behaviour of alkali activated slag and fly ash concrete: effects of hypothetical thickness, aggregates, and loading age. Mater. Struct. 58, 160.
Gunasekara, C., Atzarakis, P., Lokuge, W., Law, D.W., Setunge, S., 2021. Novel analytical method for mix design and performance prediction of high calcium fly ash geopolymer concrete. Polymers 13 (6), 900.
Gupta, T., Rao, M.C., 2022. Prediction of compressive strength of geopolymer concrete using machine learning techniques. Struct. Concr. 23 (5), 3073–3090.
Hajimohammadi, A., Ngo, T., Mendis, P., 2017. How does aluminium foaming agent impact the geopolymer formation mechanism? Cement Concr. Compos. 80, 277–286.
Hajimohammadi, A., Ngo, T., Vongsvivut, J., 2019. Interfacial chemistry of a fly ash geopolymer and aggregates. J. Clean. Prod. 231, 980–989.
Hardjito, D., Rangan, B.V., 2005. Development and Properties of Low-Calcium Fly Ash-Based Geopolymer Concrete.
He, Q., Zheng, P., Lv, X., Li, J., Li, Y., 2024. A new method for evaluating roundness error based on improved bat algorithm. Measurement 238, 115314.
Hu, Z., Dang, C., Wang, D., Beer, M., Wang, L., 2025. Error-informed parallel adaptive Kriging method for time-dependent reliability analysis. Reliab. Eng. Syst. Safe. 262, 111194.
Jia, Z., Chen, C., Zhou, H., Zhang, Y., 2020. The characteristics and formation mechanism of the dark rim in alkali-activated slag. Cement Concr. Compos. 112, 103682.
Jiang, T., Li, L., Samali, B., Yu, Y., Huang, K., Yan, W., Wang, L., 2024. Lightweight object detection network for multi-damage recognition of concrete bridges in complex environments. Comput. Aided Civ. Infrastruct. Eng. 39 (23), 3646–3665.
Jithendra, C., Elavenil, S., 2019. Role of superplasticizer on GGBS based Geopolymer concrete under ambient curing. Mater. Today Proc. 18, 148–154.
Jo, J., Jadidi, Z., 2020. A high precision crack classification system using multi-layered image processing and deep belief learning. Struct. Infrast. Eng. 16 (2), 297–305.
Kanagaraj, B., Anand, N., Lubloy, E., 2024. Sustainability and durability performance evaluation of geopolymer concrete with industrial effluent as alternative to conventional river sand. Devel. Built Environ. 19, 100517.
Karthik, A., Sudalaimani, K., Kumar, C.V., 2017. Investigation on mechanical properties of fly ash-ground granulated blast furnace slag based self curing bio-geopolymer concrete. Constr. Build. Mater. 149, 338–349.
Kaze, C.R., Adesina, A., Lecomte-Nana, G.L., Alomayri, T., Kamseu, E., Melo, U.C., 2021. Alkali-activated laterite binders: influence of silica modulus on setting time, Rheological behaviour and strength development. Clean. Eng. Technol. 4, 100175.
Kumar, S., Kumar, R., Mehrotra, S., 2010. Influence of granulated blast furnace slag on the reaction, structure and properties of fly ash based geopolymer. J. Mater. Sci. 45, 607–615.
Le, H.-B., Bui, Q.-B., Tang, L., 2021. Geopolymer recycled aggregate concrete: from experiments to empirical models. Materials 14 (5), 1180.
Le, Q.-H., Nguyen, D.-H., Sang-To, T., Khatir, S., Le-Minh, H., Gandomi, A.H., Cuong-Le, T., 2024. Machine learning based models for predicting compressive strength of geopolymer concrete. Front. Struct. Civ. Eng. 18 (7), 1028–1049.
Lee, N., Lee, H.-K., 2013. Setting and mechanical properties of alkali-activated fly ash/slag concrete manufactured at room temperature. Constr. Build. Mater. 47, 1201–1209.
Lemougna, P.N., Nzeukou, A., Aziwo, B., Tchamba, A., Wang, K.-t., Melo, U.C., Cui, X.-m., 2020. Effect of slag on the improvement of setting time and compressive strength of low reactive volcanic ash geopolymers synthetized at room temperature. Mater. Chem. Phys. 239, 122077.
Li, W., Shumuye, E.D., Shiying, T., Wang, Z., Zerfu, K., 2022. Eco-friendly fibre reinforced geopolymer concrete: a critical review on the microstructure and long-term durability properties. Case Stud. Constr. Mater. 16, e00894.
Liu, Y., Tan, X., Bao, Y., 2024. Machine learning-assisted intelligent interpretation of distributed fiber optic sensor data for automated monitoring of pipeline corrosion. Measurement 226, 114190.
Luukkonen, T., Sreenivasan, H., Abdollahnejad, Z., Yliniemi, J., Kantola, A., Telkki, V.-V., Kinnunen, P., Illikainen, M., 2020. Influence of sodium silicate powder silica modulus for mechanical and chemical properties of dry-mix alkali-activated slag mortar. Constr. Build. Mater. 233, 117354.
Memon, F.A., Nuruddin, M.F., Demie, S., Shafiq, N., 2011. Effect of curing conditions on strength of fly ash-based self-compacting geopolymer concrete. Int. J. Civ. Environ. Eng. 5 (8), 342–345.
Morsy, A.M., Ragheb, A.M., Shalan, A.H., Mohamed, O.H., 2022. Mechanical characteristics of GGBFS/FA-Based geopolymer concrete and its environmental impact. Pract. Period. Struct. Des. Construct. 27 (2), 04022017.
Nath, P., Sarker, P.K., 2014. Effect of GGBFS on setting, workability and early strength properties of fly ash geopolymer concrete cured in ambient condition. Constr. Build. Mater. 66, 163–171.
Nath, P., Sarker, P.K., 2017. Fracture properties of GGBFS-blended fly ash geopolymer concrete cured in ambient temperature. Mater. Struct. 50, 1–12.
Nedeljković, M., Li, Z., Ye, G., 2018. Setting, strength, and autogenous shrinkage of alkali-activated fly ash and slag pastes: effect of slag content. Materials 11 (11), 2121.
Ng, T.S., Foster, S.J., 2013. Development of a mix design methodology for high-performance geopolymer mortars. Struct. Concr. 14 (2), 148–156.
Nguyen, H.A.T., Pham, D.H., Ahn, Y., 2024. Effect of data augmentation using deep learning on predictive models for geopolymer compressive strength. Appl. Sci. 14 (9), 3601.
Nguyen, T.-T., Ta, Q.-B., Ho, D.-D., Kim, J.-T., Huynh, T.-C., 2023. A method for automated bolt-loosening monitoring and assessment using impedance technique and deep learning. Devel. Built Environ. 14, 100122.
Noushini, A., Aslani, F., Castel, A., Gilbert, R.I., Uy, B., Foster, S., 2016. Compressive stress-strain model for low-calcium fly ash-based geopolymer and heat-cured Portland cement concrete. Cement Concr. Compos. 73, 136–146.
Noushini, A., Castel, A., Aldred, J., Rawal, A., 2020. Chloride diffusion resistance and chloride binding capacity of fly ash-based geopolymer concrete. Cement Concr. Compos. 105, 103290.
Oyebisi, S., Alomayri, T., 2023. Artificial intelligence-based prediction of strengths of slag-ash-based geopolymer concrete using deep neural networks. Constr. Build. Mater. 400, 132606.
Pavithra, P., Reddy, M.S., Dinakar, P., Rao, B.H., Satpathy, B., Mohanty, A., 2016. A mix design procedure for geopolymer concrete with fly ash. J. Clean. Prod. 133, 117–125.
Peng, Y., Unluer, C., 2022. Analyzing the mechanical performance of fly ash-based geopolymer concrete with different machine learning techniques. Constr. Build. Mater. 316, 125785.
Reddy, D.V., Edouard, J.-B., Sobhan, K., 2013. Durability of fly ash–based geopolymer structural concrete in the marine environment. J. Mater. Civ. Eng. 25 (6), 781–787.
Roy, D.M., Adhikary, S.D., Sengupta, P., 2022. Assessment of mechanical and micro-structural characterization of novel ambient cured cement-free composite concrete. Ceram. Int. 48 (18), 26519–26538.
Shilar, F.A., Ganachari, S.V., Patil, V.B., Khan, T.Y., Khadar, S.D.A., 2022a. Molarity activity effect on mechanical and microstructure properties of geopolymer concrete: a review. Case Stud. Constr. Mater. 16, e01014.
Shilar, F.A., Ganachari, S.V., Patil, V.B., Almakayeel, N., Khan, T.Y., 2023a. Development and optimization of an eco-friendly geopolymer brick production process for sustainable masonry construction. Case Stud. Constr. Mater. 18, e02133.
Shilar, F.A., Ganachari, S.V., Patil, V.B., Bhojaraja, B., Khan, T.Y., Almakayeel, N., 2023b. A review of 3D printing of geopolymer composites for structural and functional applications. Constr. Build. Mater. 400, 132869.
Shilar, F.A., Ganachari, S.V., Patil, V.B., Nisar, K.S., 2022b. Evaluation of structural performances of metakaolin based geopolymer concrete. J. Mater. Res. Technol. 20, 3208–3228.
Shilar, F.A., Shilar, M.A., Ganachari, S.V., 2025. Advancing sustainable construction: bamboo fibers in clay-based geopolymer composites. J. Build. Eng. 104, 112247.
Siddika, A., Hajimohammadi, A., Mamun, M.A.A., Alyousef, R., Ferdous, W., 2021. Waste glass in cement and geopolymer concretes: a review on durability and challenges. Polymers 13 (13), 2071.
Singh, P.K., Rajhans, P., 2024. Influence of treated recycled concrete aggregate and modified mixing approach on the mechanical properties of ternary blend geopolymer concrete: experiments and machine learning algorithms. J. Clean. Prod. 443, 141007.
Tang, Z., Hu, Y., Tam, V.W., Li, W., 2019. Uniaxial compressive behaviors of fly ash/slag-based geopolymeric concrete with recycled aggregates. Cement Concr. Compos. 104, 103375.
Upreti, K., Verma, M., Agrawal, M., Garg, J., Kaushik, R., Agrawal, C., Singh, D., Narayanasamy, R., 2022. Prediction of mechanical strength by using an artificial neural network and random forest algorithm. J. Nanomater. 2022.
Van Jaarsveld, J., Van Deventer, J.S., Lukey, G., 2002. The effect of composition and temperature on the properties of fly ash-and kaolinite-based geopolymers. Chem. Eng. J. 89 (1–3), 63–73.
Verma, M., Dev, N., 2021. Sodium hydroxide effect on the mechanical properties of flyash-slag based geopolymer concrete. Struct. Concr. 22, E368–E379.
Verma, M., Dev, N., 2022. Effect of liquid to binder ratio and curing temperature on the engineering properties of the geopolymer concrete. Silicon 14 (4), 1743–1757.
Wang, L., Yi, S., Yu, Y., Gao, C., Samali, B., 2024a. Automated ultrasonic-based diagnosis of concrete compressive damage amidst temperature variations utilizing deep learning. Mech. Syst. Signal Process. 221, 111719.
Wang, Y., Iqtidar, A., Amin, M.N., Nazar, S., Hassan, A.M., Ali, M., 2024b. Predictive modelling of compressive strength of fly ash and ground granulated blast furnace slag based geopolymer concrete using machine learning techniques. Case Stud. Constr. Mater. 20, e03130.
Wang, Y., Liu, H., Nie, Z., Xue, R., Zhu, W., Sun, X., 2025. Experimental investigation into the influence of calcium aluminate cement on the micro-and macro-mechanical properties of the interfacial transition zone in geopolymer concrete. Devel. Built Environ., 100618
Waqas, R.M., Butt, F., Zhu, X., Jiang, T., Tufail, R.F., 2021. A comprehensive study on the factors affecting the workability and mechanical properties of ambient cured fly ash and slag based geopolymer concrete. Appl. Sci. 11 (18), 8722.
Wu, L., Zou, D., Hao, Y., 2024. Exploring the compositional effect of eco-friendly ultra-high performance concrete on dynamic strength based on stacking algorithm and explainable artificial intelligence. Devel. Built Environ. 20, 100574.
Xiao, R., Shen, Z., Si, R., Polaczyk, P., Li, Y., Zhou, H., Huang, B., 2022. Alkali-activated slag (AAS) and OPC-based composites containing crumb rubber aggregate: physico-mechanical properties, durability and oxidation of rubber upon NaOH treatment. J. Clean. Prod. 367, 132896.
Yadollahi, M.M., Benli, A., Demirboğa, R., 2015. The effects of silica modulus and aging on compressive strength of pumice-based geopolymer composites. Constr. Build. Mater. 94, 767–774.
Yang, L., An, X., Du, S., 2021. Estimating workability of concrete with different strength grades based on deep learning. Measurement 186, 110073.
Yang, X.S., Hossein Gandomi, A., 2012. Bat algorithm: a novel approach for global engineering optimization. Eng. Comput. 29 (5), 464–483.

Yi, S.-T., Yang, E.-I., Choi, J.-C., 2006. Effect of specimen sizes, specimen shapes, and placement directions on compressive strength of concrete. Nucl. Eng. Des. 236 (2), 115–127.
Yu, Y., Li, J., Li, J., Xia, Y., Ding, Z., Samali, B., 2023. Automated damage diagnosis of concrete jack arch beam using optimized deep stacked autoencoders and multi-sensor fusion. Devel. Built Environ., 100128
Yu, Y., Rashidi, M., Dorafshan, S., Samali, B., Farsangi, E.N., Yi, S., Ding, Z., 2025. Ground penetrating radar-based automated defect identification of bridge decks: a hybrid approach. J. Civil Struct. Health Monit. 15 (2), 521–543.
Yu, Y., Samali, B., Rashidi, M., Mohammadi, M., Nguyen, T.N., Zhang, G., 2022. Vision-based concrete crack detection using a hybrid framework considering noise effect. J. Build. Eng. 61, 105246.
Yuan, X., Yuan, X., Wang, X., 2021. Path planning for mobile robot based on improved bat algorithm. Sensors 21 (13), 4389.
Zandifaez, P., Shamsabadi, E.A., Nezhad, A.A., Zhou, H., Dias-da-Costa, D., 2023. AI-Assisted optimisation of green concrete mixes incorporating recycled concrete aggregates. Constr. Build. Mater. 391, 131851.
Zhang, B., Wang, Q., Zhu, H., Yang, Z., Peng, H., 2024. Behavior of BFRP-confined geopolymer-based coral aggregate concrete columns under axial compression: effects of specimen sizes. J. Build. Eng. 98, 111106.
Zhang, B., Zhu, H., Yang, Z., Dong, Y.-R., 2025a. BFRP bars reinforced geopolymer-based coral aggregate concrete beams with sustainable and high seawater erosion resistance: flexural durability, economic, and ecological analysis. Eng. Struct. 330, 119910.
Zhang, X., Cheng, L., Xu, F., Yang, C., Wang, L., 2024. A novel model for shear strength prediction of a steel–UHPC composite structure considering interface friction. J. Struct. Eng. 150 (8), 04024100.
Zhang, H., Li, L., Yuan, C., Wang, Q., Sarker, P.K., Shi, X., 2020. Deterioration of ambient-cured and heat-cured fly ash geopolymer concrete by high temperature exposure and prediction of its residual compressive strength. Constr. Build. Mater. 262, 120924.
Zhang, T., Mahdi, M., Issa, M., Xu, C., Ozevin, D., 2023. Experimental study on monitoring damage progression of basalt-FRP reinforced concrete slabs using acoustic emission and machine learning. Sensors 23 (20), 8356.
Zhang, T., Xu, C., Ozevin, D., 2025b. Acoustic emission source localization in complex pipe structure using multi-task deep learning models. Adv. Struct. Eng. 28 (1), 23–37.
Zhou, Y., Guo, Z., Zhu, Z., Ye, Z., Zhang, X., Wang, W., 2024a. Bond performance and damage assessment of self-sensing steel–fiber composite bar with geopolymer concrete. Constr. Build. Mater. 453, 138991.
Zhou, Y., Liao, X., Li, L., Guo, M., Hu, B., 2024b. Using nonionic paraffin emulsion to make waterproof engineered cementitious composites: mechanical properties and hydrophobic performance. Constr. Build. Mater. 428, 136222.
Zhou, Y., Yu, Y., Guo, W., Xing, F., Guo, M., 2024c. Development of inorganic anticorrosive coatings for steel bars: corrosion resistance testing and design. Cement Concr. Compos. 152, 105612.